HERMES: a molecular formula-oriented method to target the metabolome

Roger Giné[1], Jordi Capellades[1,2], Josep M. Badia[1,2], Dennis Vughs[3], Michaela Schwaiger-Haber[4,5], Theodore Alexandrov[6,7,8], Maria Vinaixa[1,2], Andrea M. Brunner[3], Gary J. Patti[4,5], Oscar Yanes*[1,2]

1. Universitat Rovira i Virgili, Department of Electronic Engineering & IISPV, Tarragona, Spain.
2. CIBER de Diabetes y Enfermedades Metabólicas Asociadas (CIBERDEM), Instituto de Salud Carlos III, Madrid, Spain.
3. KWR Water Research Institute, Nieuwegein, The Netherlands.
4. Department of Chemistry, Washington University, St. Louis, MO, USA.
5. Department of Medicine, Washington University, St. Louis, MO, USA.
6. Structural and Computational Biology Unit, European Molecular Biology Laboratory, Heidelberg, Germany.
7. Molecular Medicine Partnership Unit, European Molecular Biology Laboratory, Heidelberg, Germany.
8. Skaggs School of Pharmacy and Pharmaceutical Sciences, University of California San Diego, La Jolla, California, USA.

*Corresponding author:
Oscar Yanes, PhD
Department of Electronic Engineering
Universitat Rovira i Virgili
Avinguda Països Catalans, 26, 43007 Tarragona, Spain
Phone: +34 977759397
Email: oscar.yanes@urv.cat

Comprehensive metabolome analyses are essential for biomedical, environmental and biotechnological research. However, current MS1 and MS2-based acquisition and data analysis strategies in untargeted metabolomics result in low identification rates of metabolites. Here we present HERMES, a molecular formula-oriented and peak detection-free method that uses raw LC/MS1 information to optimize MS2 acquisition. Investigating environmental water, *E. coli*, and human plasma extracts with HERMES, we achieved an increased biological specificity of MS2 scans, leading to improved mass spectral similarity scoring and identification rates when compared to a state-of-the-art data-dependent acquisition (DDA) approach. Thus, HERMES improves sensitivity, selectivity and annotation of metabolites. HERMES is available as an R package with a user-friendly graphical interface for data analysis and visualization.

Introduction

A single LC/MS-based metabolomic experiment generates millions of three-dimensional (*m/z*, retention time, intensity) data points that can be annotated and quantified into thousands of metabolite features. However, most features are either redundant ions caused by ionization-related phenomena such as cation/anion adduction, multimerization and in-source fragmentation, or unknown contaminants and artifacts[1,2]. Moreover, conventional untargeted metabolomic experiments lead to highly heterogeneous chromatographic peak shapes, which negatively affect the performance of peak detection[3] and grouping/annotation algorithms in MS1 mode[4]. These characteristics of MS1 data, in turn, negatively impact MS2 acquisition methods used for metabolite identification. In data-dependent acquisition (DDA) mode, MS2 spectra are automatically collected for precursor ions that exceed a predefined intensity threshold. The selection of precursor ions is a stochastic event suffering from low analytical reproducibility and favouring the selection of the most abundant, but not necessarily biologically relevant, ions. In data-independent acquisition (DIA) methods, multiple precursor ions, including redundant and biologically irrelevant ions, are simultaneously fragmented, often generating a series of complex convoluted MS2 spectra. Despite the emergence of new software to reconstruct the link between precursors and their fragments through mass spectral deconvolution[5,6], MS2 spectral quality and matching scores to reference spectra are generally poorer in DIA compared to DDA[7].

Results

Here we present HERMES, a novel experimental method and computational tool in untargeted metabolomics that improves the selectivity and sensitivity for comprehensive metabolite profiling in MS1, and identification in MS2. HERMES replaces the conventional untargeted metabolomic workflow that detects and annotates peaks[8,9], for an inverse approach that directly interrogates raw LC/MS1 data points (within scans) by using a comprehensive list of unique molecular formulas selected by the user. These are retrieved from large compound-centric databases (e.g., HMDB, ChEBI, NORMAN)[10–12], genome-scale metabolic models, or specific metabolic pathways. Each molecular formula generates multiple 'ionic formulas' by adding or subtracting atoms from common adduct ions (Fig. 1). The resulting ionic formulas (on the order of 10^4-10^5 from a database such as HMDB) are searched against millions of data points in an LC/MS1 experiment. HERMES calculates the theoretical isotopic pattern of each ionic formula based on a predefined experimental mass resolution value (Suppl. Fig. 1). The number of collisions between monoisotopic ionic formulas vary according to the experimental mass error (i.e., the smaller the error, the larger the percentage of non-overlapping ionic formulas; Suppl. Fig. 2). An LC/MS1 data point contains *m/z* and intensity information in a wide mass range (e.g., *m/z* 80 to 1,000) for a given instant of time (Suppl. Fig 3). HERMES solves the limitations of peak detection by finding a series of scans, named SOI (Scans Of Interest), which are defined as clusters of data points that match an ionic formula, are concentrated within a short period of time and contain a minimum amount of structure determined by a 1D version of the ρ_{chaos} score from Palmer et al.[13] (see Online Methods). SOI shapes do not necessarily fit a Gaussian-like function, as assumed in basic chromatography theory, making the process independent of the heterogeneous peak shapes commonly observed in LC/MS1 experiments from complex mixtures. SOIs are then filtered in three steps: (i) blank subtraction from the sample based on an artificial neural network (Suppl. Fig. 4a), (ii) adduct and isotopologue grouping according to the similarity of their elution profiles (Suppl. Fig. 4b), and (iii) in-source fragment (ISF) annotation by using publicly available low-energy MS2 data (Suppl. Fig. 4c) extending on Domingo-Almenara et al.[14]. Finally, users can prioritize the SOIs that will constitute the inclusion list for targeted MS2 acquisition based on the following criteria: type and number of adducts, minimum intensity, isotopic fidelity, and a maximum number of overlapped precursors at any time range, which together determine the total number of MS2 runs. According to the MS2 acquisition settings, each entry in the inclusion list may be associated with one or multiple MS2 scans: if there are more than five continuous scans, HERMES provides an optional deconvolution step (adapted from CliqueMS[15]) that resolves partially co-eluting isomeric compounds (Suppl. Fig. 5); if there are fewer scans, HERMES selects the most intense scan. The resulting curated MS2 spectra

can either be identified within HERMES or exported as .mzML, .msp, or .mgf files to be used in other identification software such as NIST MS Search, SIRIUS[16,17], or GNPS[18].

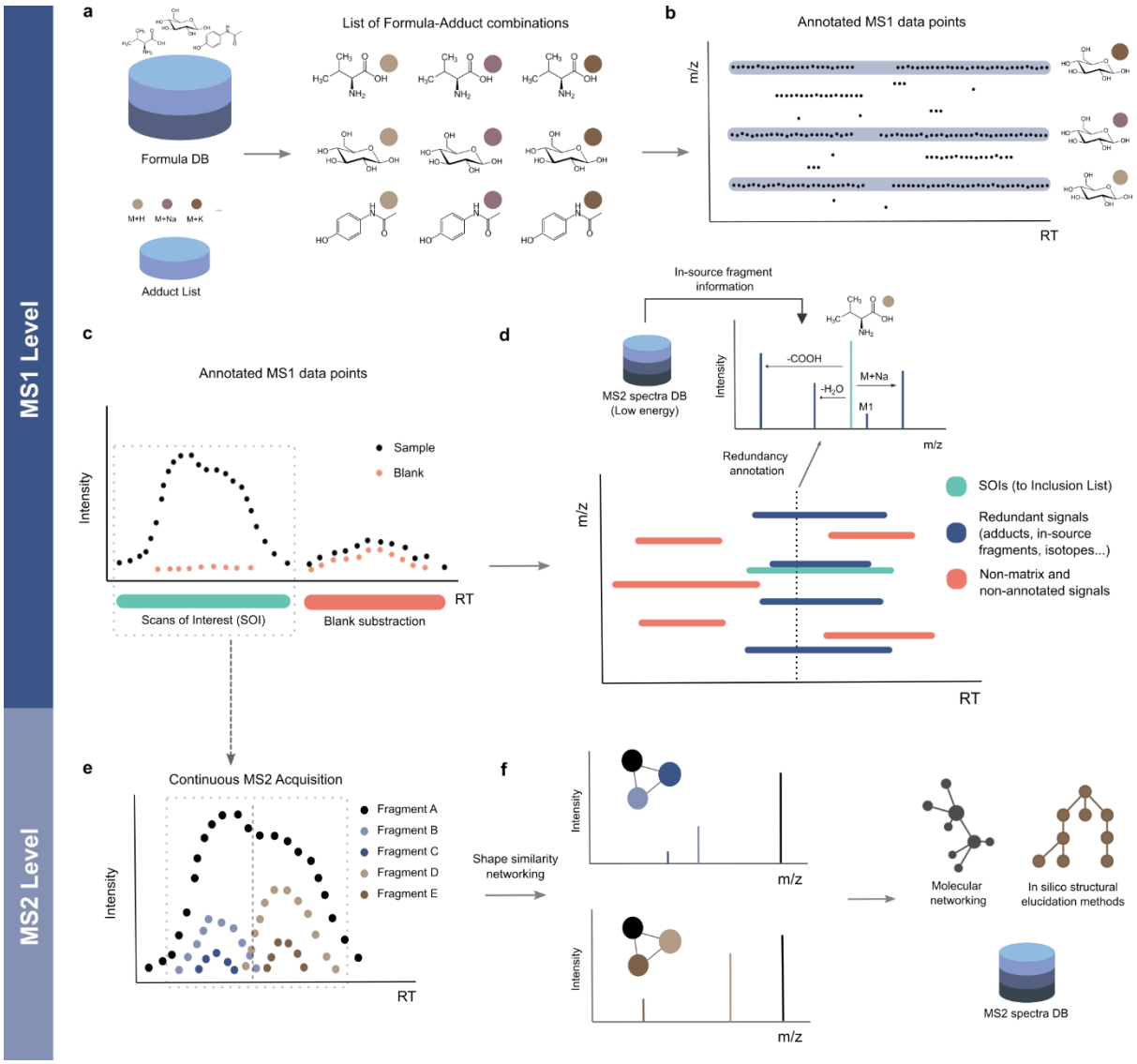

Figure 1. The HERMES workflow. (a) A context-specific database of molecular formulas and MS adducts generates a list of ionic formulas. (b) LC/MS1 data points are interrogated against all *m/z* ions corresponding to the ionic formulas and their isotopes. (c) Points with the same *m/z* annotation are grouped by density into retention time (RT) intervals called Scans of Interest (SOI). SOIs with similar shape and intensity in a blank sample are removed. (d) SOIs corresponding to different adducts of the same formula are grouped by their chromatographic elution profile. Similarly, in-source fragments are annotated based on low intensity MS2 spectra of molecules with the same formula. The result is an inclusion list (IL) of sample-specific and non-redundant precursor ions that will be monitored in a posterior MS2 experiment. (e) The IL entries are acquired continuously along the defined RT interval and HERMES groups the resulting fragment elution profiles. (f) This results in deconvoluted spectra of partially co-eluting isomeric compounds that can be queried against an MS2 database or exported to be used in alternative identification workflows.

HERMES is available as an R package (RHermes) and comes with an R Graphical User Interface (GUI) to allow data analysis, tracking of compound annotations, and visualization (Suppl. Fig. 6). RHermes accepts both CSV and XLS/XLSX files as valid molecular formula lists and can extract formulas from selected KEGG pathways for a given organism. RHermes is designed to work on ≥8GB RAM computers, however the size of the database of molecular formulas determines CPU usage and RAM memory. The running time, including blank subtraction and inclusion list generation, goes from 1 to 20 minutes on a six-core, 2.9 GHz CPU (Suppl. Table 1).

HERMES has been validated by using three (bio)chemically relevant samples of increasing complexity: (i) water collected from a canal in Nieuwegein (Netherlands), (ii) *E.coli*, and (iii) human plasma extracts. The canal water was spiked with 86 common environmental contaminants at 1 µg/L (Suppl. Table 2) and analysed by RP/LC (C18) coupled to an Orbitrap in positive (pos) and negative (neg) ionization mode operating at 120,000 resolution. HERMES detected and annotated all spiked compounds at the MS1 level using 118,820 (pos) and 46,809 (neg) ionic formulas calculated from 24,696 unique molecular formulas in the NORMAN database. Certain ionic formula collisions, particularly those involving Cl, Br, S, or K, were automatically resolved by matching experimental isotopic patterns to the expected ones. This is the case, for example, of the $[M+H]^+$ ion of chloridazon and the $[M+K]^+$ ion of 2-amino-alpha-carboline, which overlapped at 0.27 ppm (Suppl. Fig. 7). In-source fragments that could be wrongly associated with ionic formulas were also annotated by using low-energy MS2 spectra when available. The output was a curated inclusion list of 474 (pos) and 129 (neg) selective entries for targeted MS2 (Suppl. Fig. 8).

Next, a reference *E. coli* cell extract (Cambridge Isotope Laboratories) was analysed by HILIC coupled to an Orbitrap in positive and negative ionization mode. LC/MS1 data were analysed by HERMES by using 12,010 (pos) and 4,876 (neg) ionic formulas calculated from 2,463 unique molecular formulas obtained from the *Escherichia coli* Metabolome Database (ECMDB) and KEGG database. Interestingly, HERMES annotated ionic formulas for 25% (pos) and 22% (neg) of all data points acquired by the mass spectrometer (Fig. 2a and Suppl. Fig. 9a). In comparison with XCMS, a commonly used open-source LC/MS1 processing data tool in untargeted metabolomics[9,19], 16% of all acquired data points were associated with an XCMS peak, 4.3% of data points in XCMS peaks matched an ionic formula from ECMDB and KEGG database, and only 2.2% of data points in XCMS peaks were represented in the final SOI list after blank subtraction, isotopic fidelity, and ISF removal. Consequently, the overlap in isotopes and, more particularly, frequent adduct annotations between HERMES and well-established tools for annotating LC/MS1 data[15,20] was low: ~80% and <20%, respectively

(Suppl. Fig. 10a,b), showing the limitations of the peak detection strategies that have been used to date in untargeted metabolomics.

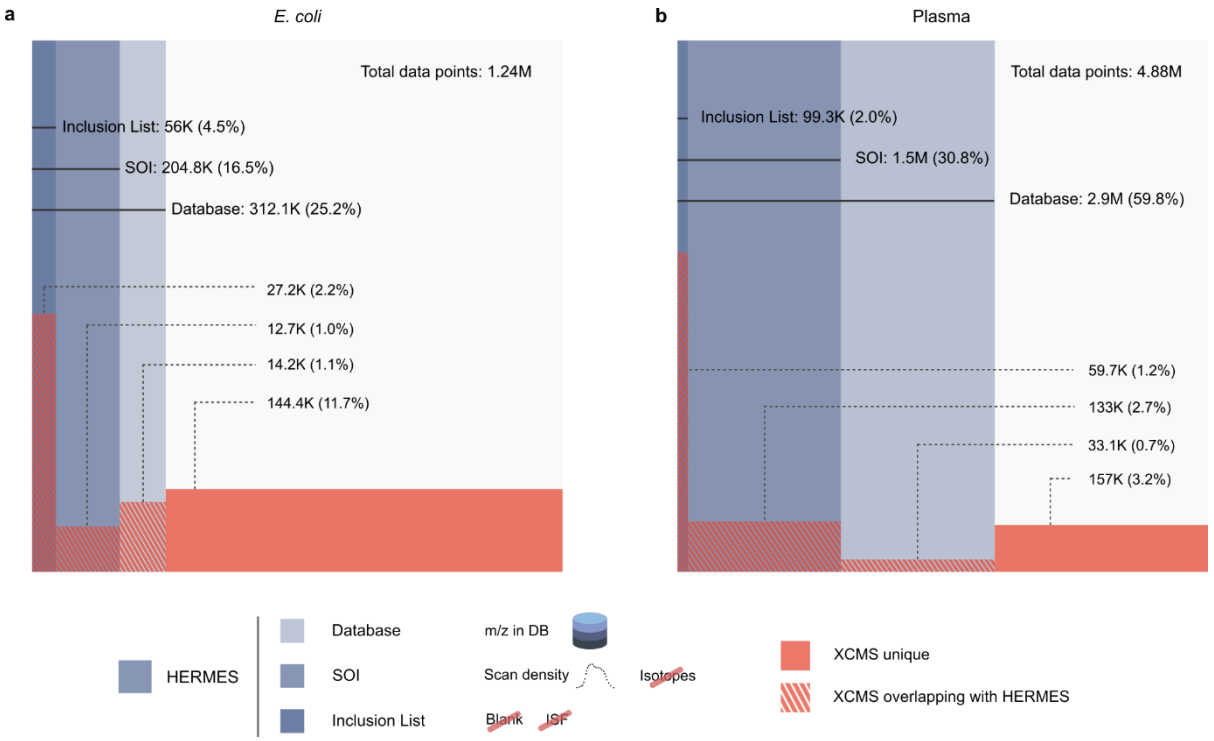

Figure 2. Venn-like diagram of the distribution of LC/MS1 data points in different steps of the HERMES workflow and XCMS peak-associated points. a) *E. coli* extract. b) Plasma extract. Database: Refers to all data points whose *m/z* matches with any *m/z* calculated from the ionic formula database (including isotopes). SOI: monoisotopic (M0)-annotated data points that are in Database and are also present in a SOI list that does not include blank subtraction nor any filtering. Inclusion List: data points present in Database and SOI kept through the blank subtraction, isotopic filter and ISF removal steps. Percentages refer to the total number of LC/MS1 data points. Positive ionization mode. On average, ~46% of data points in the inclusion list could not be annotated as a peak by XCMS. Conversely, ~86% scans annotated as a peak by XCMS could either not be matched to an ionic formula, were not specific of the sample or were associated with redundant signals.

The HERMES output was 2,058 (pos) and 1,081 (neg) SOIs that led to a curated inclusion list of 1,251 and 661 entries for targeted MS2, respectively. The *E. coli* extract was also analysed by iterative DDA under identical analytical conditions. Remarkably, 68% of DDA scans could not be annotated as the monoisotopic signal by any ionic formula from ECMDB and KEGG database (Fig. 3a), which indicates their exogenous or artefactual origin. After filtering out DDA precursor ions that were classified as SOIs in the blank sample, redundant adducts, and ISF by HERMES; only 16% of the DDA scans matched with any monoisotopic

ionic formula in the inclusion list. In addition, HERMES included 591 inclusion list entries (47% of the total) that were not triggered by DDA.

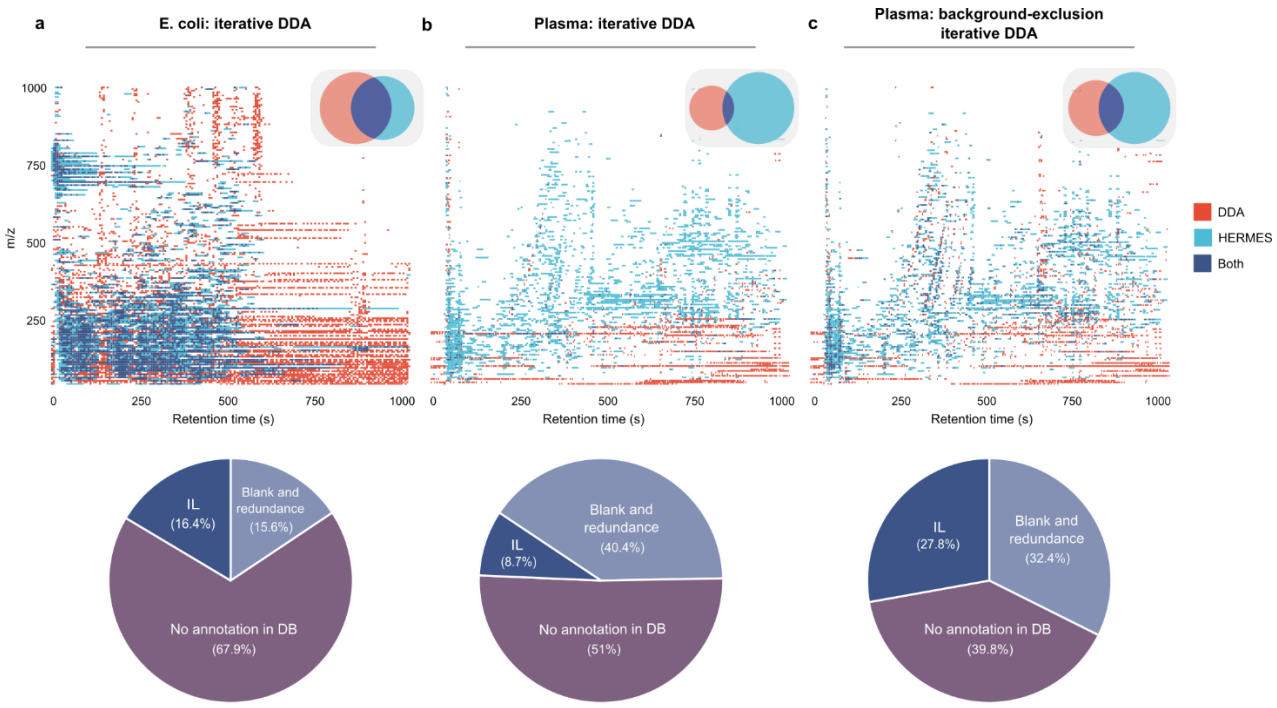

Figure 3. Distribution of MS2 scans acquired by HERMES and iterative DDA. a) Unlabelled *E. coli* and b) human plasma samples acquired by iterative DDA. c) Human plasma sample acquired by iterative DDA with background-exclusion. The acquired scans have been binned into 5Da-5s intervals. The Venn diagrams show the bin intersections between HERMES and DDA. The precursor *m/z* of DDA scans have been queried into the corresponding ionic formula *m/z* database with a 3 ppm mass error tolerance. DDA scans annotated in the database were further classified according to whether the *m/z* and retention time of the scans could be matched to the HERMES inclusion list or not. Percentages in the pie-charts refer to the total number of acquired DDA MS2 scans.

To confirm the biogenic specificity of the MS2 scans in HERMES, a reference ^{13}C-labeled (at ≥98% from uniformly ^{13}C-labeled glucose) *E. coli* credentialing extract was analysed under identical LC/MS1 conditions. For each selected precursor ion in the unlabelled *E.coli* sample, we calculated its fractional contribution (FrC)[21–23] and the monoisotopic ratio score (MIRS) by using the analogue ^{13}C-labeled sample (see Online Methods). A metabolite with *n* carbon atoms can have zero (FrC=0) to *n* (FrC=1) of its carbon atoms labelled with ^{13}C. In turn, similar intensity of the monoisotopic ion in the unlabelled and ^{13}C-labelled *E. coli* extracts indicates no isotopic enrichment (MIRS=0), whereas loss of intensity in the ^{13}C-labelled sample is associated with enrichment (MIRS=1). Around 63% of inclusion list entries in HERMES were associated with highly ^{13}C-enriched metabolites (FrC and MIRS>0.5),

proving the biosynthetic origin of these ions (Fig. 4a-c)[24]. These are mainly associated with abundant ions, while unlabelled precursors relate more frequently to low-abundant ions (Suppl. Fig. 11a,b). In contrast, only 20% of all DDA scans were associated with ^{13}C-labeled and annotated precursors from ECMDB and the KEGG database, pointing to ions also present in the blank sample as the main source of unlabelled precursors (Fig. 4d-f). ^{13}C-labeled precursors in DDA corresponded to highly abundant ions that were also covered by inclusion list entries in HERMES (Suppl. Fig. 11c).

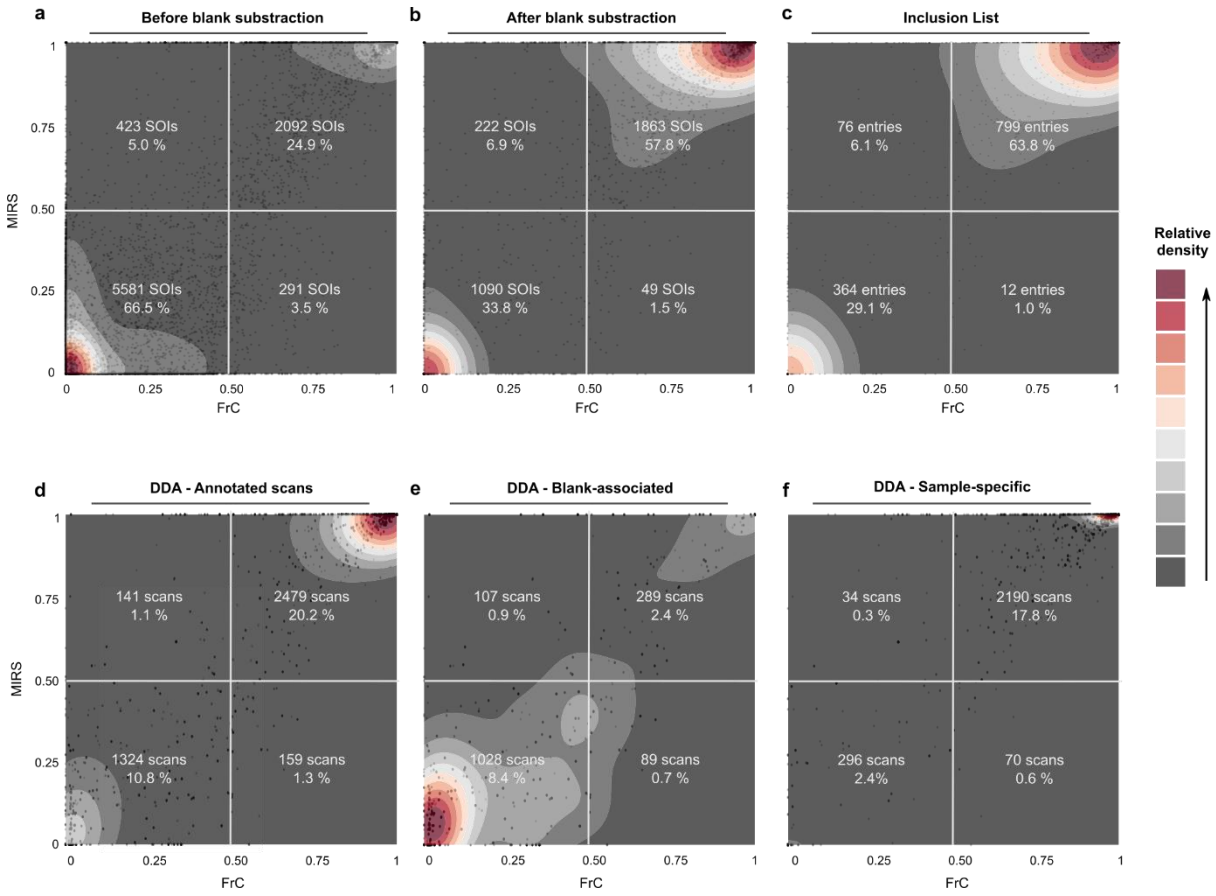

Figure 4. ^{13}C-enrichment analysis in the labelled *E. coli* sample. Each panel represents a scatterplot of two independent isotopic enrichment scores ─ FrC (Fractional Contribution) and MIRS (MonoIsotopic Ratio Score) ─ and an overlaid density estimation. a) Distribution of SOIs before applying the blank subtraction filtering in HERMES. b) Same SOI list after removing most blank-related SOIs. c) SOIs in the MS2 inclusion list after removing redundant signals from b). d) Iterative DDA scans that could be matched to any *m/z* of the ionic formula database. e) DDA scans associated with SOIs removed during the blank subtraction step from a) to b). f) DDA scans associated with SOIs conserved during the blank subtraction. Percentages in a), b) and c) correspond to the total number of SOIs and inclusion list entries, accordingly, while percentages in d), e) and f) correspond to the total number of acquired DDA scans.

The biogenic specificity of HERMES resulted in higher similarity scores by mass spectral matching in databases (MassBankEU, MoNA, HMDB, Riken, NIST14, mzCloud)[25] than iterative DDA (see Online Methods). HERMES provided nearly double the number of confident structural metabolite annotations than iterative DDA (Fig. 5a and Suppl. Fig. 12a). The higher identification rate of HERMES was validated by using alternative spectral similarity and distance metrics (Suppl. Fig. 13). A fraction of the ^{13}C-labeled compounds, however, could not be identified due to low intensity SOIs and/or the lack of reference spectra in databases. For the former, setting the maximum ion injection time at high values (1,500 ms) improved sensitivity and MS2 spectral quality in HERMES, resulting in more informative fragments and better spectral matching (Suppl. Fig. 14). Furthermore, we identified unlabelled metabolites (FrC=0) in the ^{13}C-labeled *E.coli* sample, such as choline, that we attribute to contaminants of the minimal growth medium that could not properly be removed by blank subtraction.

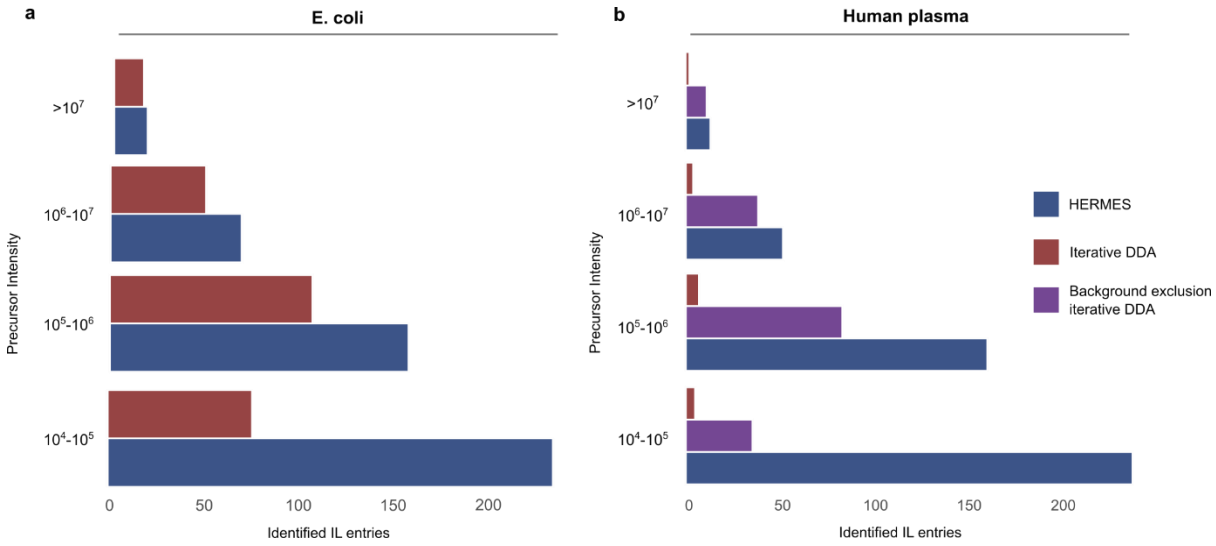

Figure 5. **Identified inclusion list entries according to the MS1 precursor intensity.** An inclusion list (IL) entry is considered identified if at least one MS2 scan associated with it has a compound hit in the reference MS2 database with either cosine score > 0.8 (in-house database from MassBankEU, MoNA, Riken and NIST14 spectra), or Match > 90 and Confidence > 30 (mzCloud). Positive ionization data. a) *E. coli* extract. b) Human plasma extract.

Finally, we used a human plasma extract to compare HERMES and iterative DDA, with and without background exclusion[26]. Here we used 23,797 unique molecular formulas from the HMDB and Chemical Entities of Biological Interest (ChEBI) database to explore virtually all known exogenous and endogenous small molecules in this biofluid. HERMES generated 110,387 and 46,973 ionic formulas that covered 60% and 14% of all data points acquired by

LC (RPC18)-Orbitrap MS in positive and negative ionization mode, respectively (Fig. 2b and Suppl. Fig 9b). Consistent with the pattern observed for *E. coli*, 8% of all acquired data points were associated with an XCMS peak (Fig. 2b), which resulted in less than 10% overlap of the most frequent adducts annotations between HERMES and CliqueMS/CAMERA (Suppl. Fig. 10c,d). Only 1.2% of the data points in XCMS peaks matched with an ionic formula from HMDB or ChEBI and were present in the inclusion list. Again, more than half of DDA precursors could not be annotated as monoisotopic ionic formulas from HMDB and ChEBI without blank subtraction (Fig. 3b). As expected, background exclusion in iterative DDA increased to 28% the number of common MS2 scans between HERMES and DDA (Fig. 3c). Yet, the number of confident structural metabolite identifications with HERMES was more than three times greater than DDA because of the larger coverage of sample-specific and low abundant precursor ions (Fig. 5b and Suppl. Fig. 12b).

Discussion

Our results demonstrate that a conventional LC/MS-based untargeted metabolomic experiment can contain up to ~50 times more non-specific and redundant data points than sample-specific and selective ones, which can account for as much as 90% of the MS2 acquisition run time in a state-of-the-art iterative DDA experiment. Current untargeted metabolomic approaches are unable to properly annotate the large number of 'junk' MS1 and MS2 signals, leading to low-quality MS2 spectra, false-positive identifications and an overall low number of identified metabolites. HERMES solves this problem by implementing a broad scope and molecular formula-oriented method that improves MS2 coverage by optimizing MS2 acquisition time focusing on sample-specific, MS1 pre-annotated, and biologically relevant compounds. In contrast to DDA, the continuous targeted MS2 acquisition in HERMES does not acquire MS1 scans nor use dynamic exclusion, allowing a cleaner and easier deconvolution and thereby increasing the quality of MS2 spectra and the number of identified metabolites. This is also a differentiating element compared to DIA, where multiple precursor ions, including redundant and biologically irrelevant ions, are simultaneously fragmented.

Although HERMES relies on high resolution MS data, it can be applied to the full range of HRMS instrumentations and mass resolutions. We tested HERMES using an LC-QTOF MS at ~30.000 resolution with the only drawback that certain isotopic patterns were difficult to annotate due to lower isotopic fidelity and possible interferences, as shown in Suppl. Fig. 1.

The coverage of compounds detected by HERMES in any given sample is determined by the list of molecular formulas. We currently provide ready-to-use lists for most important

databases in biomedical and/or environmental studies: HMDB, ChEBI, NORMAN, KEGG, LipidMaps[27] and LipidBlast[28], which can be used individually or merged in a customized way, leading to >10^3-10^4 unique molecular formulas. Yet, HERMES provides maximum experimental flexibility by allowing users to add new molecular formulas not reported in public databases[29], including *in silico* secondary metabolism prediction[30–32] such as environmental microbial degradation, biotransformations of gut and soil/aquatic microbiota, or small peptides such as dipeptides and tripeptides. Therefore, in a context where virtually all known molecular formulas (>10^3-10^4) can be covered, we believe that 'untargeted' and 'broad scope targeted' are interchangeable terms to define HERMES.

Future developments should provide optimized maximum ion injection time and collision energies for each inclusion list entry to reduce the number of MS2 scans required, and improve the quality of MS2 spectra, particularly for low intensity SOIs. Also, the ability to annotate in-source fragments by HERMES is determined by the size and content of public (and in-house) MS2 databases. In-source fragments from metabolites that are not present in a MS2 database, or do not contain low-energy MS2 data, will not be annotated. As a rough guide, we currently filter out ~10% of the SOIs as in-source fragments, however, this percentage may change as more metabolites are added to MS2 databases. Finally, the use of sample-specific and high-quality MS2 spectra linked to preannotated precursor ions (i.e., molecular formula, adduct) should restrict the range of known and unknown chemical structures for *in silico* MS2 fragmentation tools. This includes the possibility to find unknown isomeric forms from known molecular formulas, provided that these novel structural isomers produce sufficiently specific fragmentation spectra.

Online Methods

Materials. LC/MS-grade acetonitrile, water, isopropanol, and methanol (Burdick & Jackson) were purchased from Honeywell (Muskegon, MI). LC/MS-grade ammonium bicarbonate, ammonium hydroxide and methylenediphosphonic (medronic) acid were purchased from Sigma-Aldrich (St. Louis, MO). Dried down metabolic extracts of *E. coli* were purchased from Cambridge Isotope Laboratories (MSK-CRED-DD-KIT). Spike-in compounds (Suppl. Table 1) were purchased from Sigma-Aldrich (Zwijndrecht, The Netherlands), LGC Standards (Wesen, Germany) and Toronto Research Chemicals (Toronto, ON).

Sample preparation

Environmental water. Surface water was obtained from the Lekkanaal at Nieuwegein (The

Netherlands). The spike-in compounds were added to the surface water sample to a final concentration of 1 µg/L. Subsequently, the sample was filtered using Phenex™ reversed cellulose 15 mm Syringe Filters 0.2u (Phenomenex, Torrance, USA) and transferred to a LC autosampler vial.

E.coli. Dried down *E. coli extracts (*unlabelled and uniformly ^{13}C-labelled) were reconstituted in 100 µL of acetonitrile:water (2:1), followed by 30 s vortexing, 5 min of sonication, and 30 s of vortexing.

Human plasma. Plasma aliquots (50 µL) were thawed at 4ºC and briefly vortex-mixed. Proteins were precipitated by the addition of 200 µL cold acetonitrile/methanol/water (5:4:1, vol/vol) followed by 10 seconds vortex-mixing. Samples were subsequently maintained on ice for 30 min. After centrifugation (10 min, 15.200 rpm at 4ºC), 100 µL of supernatant were transferred to a LC autosampler vial.

LC-MS analysis

Environmental water and human plasma. Ultra-high performance LC (UHPLC)/MS was performed with a Thermo Scientific Vanquish UHPLC system interfaced with a Thermo Scientific Orbitrap Fusion Tribrid mass spectrometer operated in positive or negative ion mode. Reverse phase C18 liquid chromatography (RPLC) analysis was performed by using a Xbridge BEH C18 column (Waters, Etten-Leur, The Netherlands) with the following specifications: 150 mm x 2.1 mm, 2.5 µm. Mobile-phase solvents were composed of A = ultrapure water with 0.05% formic acid (v/v) and B = acetonitrile with 0.05% formic acid (v/v). The column compartment was maintained at 25 °C for all experiments. The following linear gradient was applied at a flow rate of 250 µL/min: 0-1 min: 5% B, 1-25 min: 5-100% B, 25-29 min: 100% B, 29.0-29.5 min 5% B followed by 4.5 min of re-equilibration phase. One µL of the human plasma extract was diluted in 100 µL of ultrapure water, and the injection volume was 100 µL for all experiments. Data were collected with the following settings: spray voltage, 3.0 kV and -2.5 kV in positive and negative mode, respectively; sheath gas, 40; auxiliary gas, 10; sweep gas, 5; ion transfer tube temperature, 300 °C; vaporizer temperature, 300 °C; mass range, 80-1000 Da; RF lens, 50%; resolution, 120,000 (MS1), 15,000 (MS2); AGC target, 2e5 (MS1), 5e4 (MS2); maximum injection time, 100 ms (MS1), 50 ms (HERMES), 50 ms (DDA); isolation window, 1.6 Da. The collision energy was 35% for HCD fragmentation. With every batch run, mass calibration was performed using Pierce ESI positive and negative ion calibration solution to obtain a mass error of <2 ppm.

E.coli. LC/MS was performed with a Thermo Scientific Vanquish Horizon UHPLC system interfaced with a Thermo Scientific Orbitrap ID-X Tribrid Mass Spectrometer (Waltham, MA). Hydrophilic interaction liquid chromatography (HILIC) analysis was performed by using a

SeQuant ZIC-pHILIC column (Merck Millipore, Burlington, MA) with the following specifications: 150 mm x 2.1 mm, 5 µm. Mobile-phase solvents were composed of A = 20 mM ammonium bicarbonate, 0.1% ammonium hydroxide solution (25% ammonia in water) and 2.5 µM medronic acid in water:acetonitrile (95:5) and B = 95% acetonitrile, 5% water, 2.5 µM medronic acid. The column compartment was maintained at 40 ^{o}C for all experiments. The following linear gradient was applied at a flow rate of 250 µL min-1: 0-1 min: 90% B, 1-12 min: 90-35% B, 12.5-14.5 min: 25% B, 15 min: 90% B followed by 4 min of re-equilibration phase at 400 µL min-1 and 2 min at 250 µL min-1. The injection volume was 2 µL for all experiments. Data were collected with the following settings: spray voltage, 3.5 kV and -2.8 kV in positive and negative mode, respectively; sheath gas, 50; auxiliary gas, 10; sweep gas, 1; ion transfer tube temperature, 300 °C; vaporizer temperature, 200 °C; mass range, 70-1000 Da; RF lens, 60%; resolution, 120,000 (MS1), 15,000 (MS2); AGC target, 2e5 (MS1), 5e4 (MS2); maximum injection time, 200 ms (MS1), 35 ms (HERMES, unless otherwise stated), 100 ms (iterative DDA); isolation window, 1 Da. The collision energy was 35% for HCD fragmentation.

Iterative DDA

E.coli. After the first DDA run, the raw data file containing MS2 spectra was converted to an .MS2 file using MS Convert[33] Next, the IEomics tool[34] was used to generate the first exclusion list of features fragmented in the first DDA run. User inputs in the R script were RTWindow = 0.3 min, noiseCount = 25, MZWindow = 0.001. This procedure was repeated two times, which resulted in a total of three DDA data runs per polarity. The mass tolerance for exclusion lists was 5 ppm.

Plasma. An exclusion list of background ions was generated using the AcquireX workflow of Xcalibur data acquisition software (Thermo Fisher Scientific), by analysing an ultrapure water sample. The exclusion list contains the exact mass, retention window and intensity (exclusion override factor = 3) of the excluded background ions. DDA was per performed for the top 6-8 most intense ions per full scan. Dynamic exclusion was used to prevent redundant acquisition of MS2 spectra for a selected precursor ion for 10 s, when two MS2 spectra were acquired within 20 s, resulting in a total of three DDA data runs per polarity. A mass tolerance of 5 ppm was used for the exclusion list and dynamic exclusion.

HERMES algorithm

All analysis were performed using RHermes (version 0.99.0).

MS1 data processing: Theoretical isotopic patterns of each ionic formula were calculated by Envipat (version 2.4) and refined by RHermes, based on the predefined experimental mass

resolution and mass accuracy values. Local resolution was calculated for each ionic formula as: $R(mz) = R_{ref} \cdot \sqrt{\frac{mz}{mz_{ref}}}$.

Using as input a set of mzML files, SOIs were detected by RHermes using two sets of 5s bins (offset by 2.5s) and required a minimum scan density of 30% of acquired scans.

Blank subtraction was performed using an heuristic prefilter (intensity ratio sample/blank > 3) and an artificial neural network (ANN) trained with >3000 manually annotated sample/blank SOI comparisons from two different biological matrices. Each blank-sample pair was manually classified according to whether the elution shape and intensity were similar (0) or not (1). The entries were then separated into 80/20 training and testing sets. The model was trained using Keras (https://keras.io/), with the categorical crossentropy metric as a performance indicator. After XXXXX rounds of training, the model obtained a XX% accuracy in the testing set. Adduct and isotopologue grouping were performed using a cosine shape similarity score and required a cosine >0.8. Cosine similarity has a superior discriminatory power than the Pearson correlation[13] for discriminating between features corresponding to the same metabolite from coeluting features corresponding to different metabolites[15].

In-source fragment (ISF) annotation was performed using an in-house MS2 database consisting of 675,663 low-energy spectra (<20% HCD, <10eV CID) from MassBankEU, MoNA, HMDB, Riken and NIST14. Low-energy spectra were selected according to each SOI formula annotation. Intense (>20% of maximum intensity) fragments *m/z* were then queried against the SOI list. Finally, the suspected ISF SOIs elution profiles were compared to the original SOI and a cosine similarity score was calculated.

MS2 data processing. The program exports the inclusion list into a csv file used to generate the MS2 acquisition method. Acquired MS2 scans were linked to each inclusion list entry; if >5 scans were acquired, a deconvolution algorithm was applied, where fragments *m/z* were grouped and initially split with a Centwave peak picking (peakwidth = c(5,60)). A cosine shape similarity score was applied to each pair of fragment peaks to generate a similarity network. Each network was then partitioned using a greedy algorithm from *igraph* (version 1.2.4.2) and yielded a variable number of deconvoluted MS2 spectra (see Algorithm 3). If fewer than 5 scans were acquired, the scan with the highest TIC was selected and filtered by intensity (> 0.5% of maximum).

Note: the program can also process conventional DDA data to filter out blank-related MS2 scans. RHermes uses DDA's MS1 scans to generate a SOI list and uses only those MS2 scans that match with the SOI list.

XCMS data processing

LC/MS1 raw data files (ESI+ and ESI− modes) were converted to open standard format mzML using Proteowizard MS-convert[33] and subsequently processed by HERMES and XCMS software[19] (version 3.8.1). XCMS settings were: xcmsSet(method="centWave", ppm=3, peakwidth=c(10, 60)); Common data points between SOIs in HERMES and XCMS peaks were calculated by extracting the raw data points delimited by each XCMS peak ($rt_{min} < rt < rt_{max}$ and $mz_{min} < mz < mz_{max}$) and generating the set intersections using *dplyr* (version 1.0.4).

CAMERA and CliqueMS data processing

Both CAMERA and CliqueMS were run using their respective default adduct lists, which contained all adducts considered by HERMES. Mass error for both tools was set to 3 ppm.

Uniformly ^{13}C-labeled *E. coli*

Fractional contribution (FrC) was calculated using the formula:

$$FrC = \sum_{i=1}^{N} \frac{M_i \cdot i}{M0_{unlab} \cdot n}$$

where N is the number of carbon atoms in the molecule.

MonoIsotopic Ratio Score (MIRS) was calculated using the formula:

$$MIRS = 1 - \frac{M0_{labelled}}{M0_{unlabelled}}$$

If MIRS was smaller than zero, it was set to zero so that all points range from 0 to 1.

MS2 identification

In-house DB. MS2 spectra were obtained from MassBankEU, MoNA, HMDB, Riken and NIST14 databases. RHermes includes the MassBank EU database for testing purposes, which is available as an .rds file at Zenodo (accession number 4678268).

All fragment *m/z* were discretized into 0.01Da bins. Each spectrum precursor *m/z* was matched against the DB spectra *m/z* with a 0.01Da tolerance. For the HERMES matching, the reference spectra were further filtered according to the formula database used in the MS1 analysis. A cosine similarity score was calculated between the query and reference spectra and resulting hits were filtered by requiring a score > 0.8.

mzCloud DB. The processed HERMES MS2 spectra were exported to the mzML file format. The DDA files were directly imported through MassFrontier version 8.0 SR1 (Thermo Scientific) and matched against the mzCloud database using three component identification types: Identity, Similarity Forward and Similarity Reverse; with the following constraints: 4.0

Tolerance Factor and Match Ion Activation Type. The resulting hits were filtered by both Match and Confidence scores (requiring a score > 90 and > 30, respectively).

Identified inclusion list entries (Figure 5 and Supp Figure 11) were calculated as number of inclusion list entries that resulted in a valid hit (i.e. high score) against either of the two databases. For DDA, this number was calculated by matching the precursor *m/z* and RT of the scans to the inclusion list and then examining if (i) any of the scans have at least one valid hit against either of the two databases and (ii) any valid hit had a molecular formula present in the HERMES formula database.

All similarity metrics were calculated using the R package philentropy (version 0.4.0). MS2 spectra were discretized into 0.01Da bins and their fragment intensities scaled by the sum of the intensities, so that all calculated metrics were comparable across the spectra. The query spectra (both DDA and HERMES) were matched against the previously described In-house DB. For each query, all DB hits were grouped, taking the maximum similarity (cosine and fidelity) and the lowest distance (squared chord and topsoe). Additionally, HERMES hits were restricted to compounds with formulas present in the HERMES formula database. The corresponding plots were generated using ggplot2 (version 3.3.3).

Data availability

Input mzML/mzXML mass spectrometry data files and an RMarkdown are available at Zenodo with the accession number 4678268.

Code availability

The source code of RHermes is offered to the public as a freely accessible software package under the GNU GPL, version 3 license, and is available at https://github.com/RogerGinBer/RHermes.

Acknowledgements

We gratefully acknowledge financial support by Ministerio de Educación y Formación Profesional (Spanish Government) to R.G. (2020-COLAB-00552). O.Y. was supported by Ministerio de Economía y Competitividad (MINECO) (BFU2014-57466-P), Spanish Biomedical Research Centre in Diabetes and Associated Metabolic Disorders (CIBERDEM), an initiative of Instituto de Investigación Carlos III (ISCIII), and the European Union's Horizon 2020 program (MSCA-ITN-2015; 675610). We thank members of the Mil@b for helpful comments.

Author contributions

RG and OY designed the research. RG, JC, JMB, MV and OY developed the computational method. DV and MSH performed LC-MS and MS2 experiments. All authors applied and evaluated the method on biological samples. RG and OY wrote the manuscript, in cooperation with all authors.

Competing interests

The authors declare no personal financial interests. A patent application for the method has been filled by RG, JC and OY (P202030061).

References

1. Sindelar, M. & Patti, G. J. Chemical Discovery in the Era of Metabolomics. *J. Am. Chem. Soc.* **142**, 9097–9105 (2020).
2. Duan, L., Molnár, I., Snyder, J. H., Shen, G. & Qi, X. Discrimination and Quantification of True Biological Signals in Metabolomics Analysis Based on Liquid Chromatography-Mass Spectrometry. *Mol. Plant* **9**, 1217–1220 (2016).
3. Myers, O. D., Sumner, S. J., Li, S., Barnes, S. & Du, X. Detailed Investigation and Comparison of the XCMS and MZmine 2 Chromatogram Construction and Chromatographic Peak Detection Methods for Preprocessing Mass Spectrometry Metabolomics Data. *Anal. Chem.* **89**, 8689–8695 (2017).
4. Domingo-Almenara, X., Montenegro-Burke, J. R., Benton, H. P. & Siuzdak, G. Annotation: A Computational Solution for Streamlining Metabolomics Analysis. *Anal. Chem.* **90**, 480–489 (2018).
5. Tsugawa, H. *et al.* MS-DIAL: data-independent MS/MS deconvolution for comprehensive metabolome analysis. *Nat. Methods* **12**, 523–526 (2015).
6. Yin, Y., Wang, R., Cai, Y., Wang, Z. & Zhu, Z.-J. DecoMetDIA: Deconvolution of Multiplexed MS/MS Spectra for Metabolite Identification in SWATH-MS-Based Untargeted Metabolomics. *Anal. Chem.* **91**, 11897–11904 (2019).

7. Guo, J. & Huan, T. Comparison of Full-Scan, Data-Dependent, and Data-Independent Acquisition Modes in Liquid Chromatography–Mass Spectrometry Based Untargeted Metabolomics. *Anal. Chem.* **92**, 8072–8080 (2020).
8. Röst, H. L. *et al.* OpenMS: a flexible open-source software platform for mass spectrometry data analysis. *Nat. Methods* **13**, 741–748 (2016).
9. Huan, T. *et al.* Systems biology guided by XCMS Online metabolomics. *Nat. Methods* **14**, 461–462 (2017).
10. Wishart, D. S. *et al.* HMDB 4.0: the human metabolome database for 2018. *Nucleic Acids Res.* **46**, D608–D617 (2018).
11. J, H. *et al.* ChEBI in 2016: Improved services and an expanding collection of metabolites. *Nucleic Acids Res.* **44**, D1214-9 (2015).
12. NORMAN Network *et al.* S0 | SUSDAT | Merged NORMAN Suspect List: SusDat. (2020) doi:10.5281/zenodo.4249026.
13. Palmer, A. *et al.* FDR-controlled metabolite annotation for high-resolution imaging mass spectrometry. *Nat. Methods* **14**, 57–60 (2017).
14. Domingo-Almenara, X. *et al.* Autonomous METLIN-Guided In-source Fragment Annotation for Untargeted Metabolomics. *Anal. Chem.* **91**, 3246–3253 (2019).
15. Senan, O. *et al.* CliqueMS: a computational tool for annotating in-source metabolite ions from LC-MS untargeted metabolomics data based on a coelution similarity network. *Bioinformatics* **35**, 4089–4097 (2019).
16. Dührkop, K. *et al.* SIRIUS 4: a rapid tool for turning tandem mass spectra into metabolite structure information. *Nat. Methods* **16**, 299–302 (2019).
17. Dührkop, K. *et al.* Systematic classification of unknown metabolites using high-resolution fragmentation mass spectra. *Nat. Biotechnol.* 1–10 (2020) doi:10.1038/s41587-020-0740-8.
18. Aron, A. T. *et al.* Reproducible molecular networking of untargeted mass spectrometry data using GNPS. *Nat. Protoc.* **15**, 1954–1991 (2020).

19. Smith, C. A., Want, E. J., O'Maille, G., Abagyan, R. & Siuzdak, G. XCMS: Processing Mass Spectrometry Data for Metabolite Profiling Using Nonlinear Peak Alignment, Matching, and Identification. *Anal. Chem.* **78**, 779–787 (2006).
20. Kuhl, C., Tautenhahn, R., Böttcher, C., Larson, T. R. & Neumann, S. CAMERA: An Integrated Strategy for Compound Spectra Extraction and Annotation of Liquid Chromatography/Mass Spectrometry Data Sets. *Anal. Chem.* **84**, 283–289 (2012).
21. Buescher, J. M. *et al.* A roadmap for interpreting 13C metabolite labeling patterns from cells. *Curr. Opin. Biotechnol.* **34**, 189–201 (2015).
22. Zamboni, N., Saghatelian, A. & Patti, G. J. Defining the Metabolome: Size, Flux, and Regulation. *Mol. Cell* **58**, 699–706 (2015).
23. Jang, C., Chen, L. & Rabinowitz, J. D. Metabolomics and Isotope Tracing. *Cell* **173**, 822–837 (2018).
24. Mahieu, N. G., Huang, X., Chen, Y.-J. & Patti, G. J. Credentialing Features: A Platform to Benchmark and Optimize Untargeted Metabolomic Methods. *Anal. Chem.* **86**, 9583–9589 (2014).
25. Vinaixa, M. *et al.* Mass spectral databases for LC/MS- and GC/MS-based metabolomics: State of the field and future prospects. *TrAC Trends Anal. Chem.* **78**, 23–35 (2016).
26. Cho, K. *et al.* Targeting unique biological signals on the fly to improve MS/MS coverage and identification efficiency in metabolomics. *Anal. Chim. Acta* **1149**, 338210 (2021).
27. Fahy, E., Sud, M., Cotter, D. & Subramaniam, S. LIPID MAPS online tools for lipid research. *Nucleic Acids Res.* **35**, W606-612 (2007).
28. Kind, T. *et al.* LipidBlast in silico tandem mass spectrometry database for lipid identification. *Nat. Methods* **10**, 755–758 (2013).
29. Ludwig, M. *et al.* Database-independent molecular formula annotation using Gibbs sampling through ZODIAC. *Nat. Mach. Intell.* **2**, 629–641 (2020).

30. Djoumbou-Feunang, Y. *et al.* BioTransformer: a comprehensive computational tool for small molecule metabolism prediction and metabolite identification. *J. Cheminformatics* **11**, 2 (2019).
31. Rutz, A. *et al.* Open Natural Products Research: Curation and Dissemination of Biological Occurrences of Chemical Structures through Wikidata. *bioRxiv* 2021.02.28.433265 (2021) doi:10.1101/2021.02.28.433265.
32. Blin, K. *et al.* antiSMASH 5.0: updates to the secondary metabolite genome mining pipeline. *Nucleic Acids Res.* **47**, W81–W87 (2019).
33. Chambers, M. C. *et al.* A cross-platform toolkit for mass spectrometry and proteomics. *Nat. Biotechnol.* **30**, 918–920 (2012).
34. Koelmel, J. P. *et al.* Expanding Lipidome Coverage Using LC-MS/MS Data-Dependent Acquisition with Automated Exclusion List Generation. *J. Am. Soc. Mass Spectrom.* **28**, 908–917 (2017).

Supplementary File

HERMES: a molecular formula-oriented method to target the metabolome

Roger Giné[1], Jordi Capellades[1,2], Josep M. Badia[1,2], Dennis Vughs[3], Michaela Schwaiger-Haber[4,5], Theodore Alexandrov[6,7,8], Maria Vinaixa[1,2], Andrea M. Brunner[3], Gary J. Patti[4,5], Oscar Yanes*[1,2]

1. Universitat Rovira i Virgili, Department of Electronic Engineering & IISPV, Tarragona, Spain.
2. CIBER de Diabetes y Enfermedades Metabólicas Asociadas (CIBERDEM), Instituto de Salud Carlos III, Madrid, Spain.
3. KWR Water Research Institute, Nieuwegein, The Netherlands.
4. Department of Chemistry, Washington University, St. Louis, MO, USA.
5. Department of Medicine, Washington University, St. Louis, MO, USA.
6. Structural and Computational Biology Unit, European Molecular Biology Laboratory, Heidelberg, Germany.
7. Molecular Medicine Partnership Unit, European Molecular Biology Laboratory, Heidelberg, Germany.
8. Skaggs School of Pharmacy and Pharmaceutical Sciences, University of California San Diego, La Jolla, California, USA.

*Corresponding author:
Oscar Yanes, PhD
Department of Electronic Engineering
Universitat Rovira i Virgili
Avinguda Països Catalans, 26, 43007 Tarragona, Spain
phone: +34 977759397
email: oscar.yanes@urv.cat

Supplementary Figures

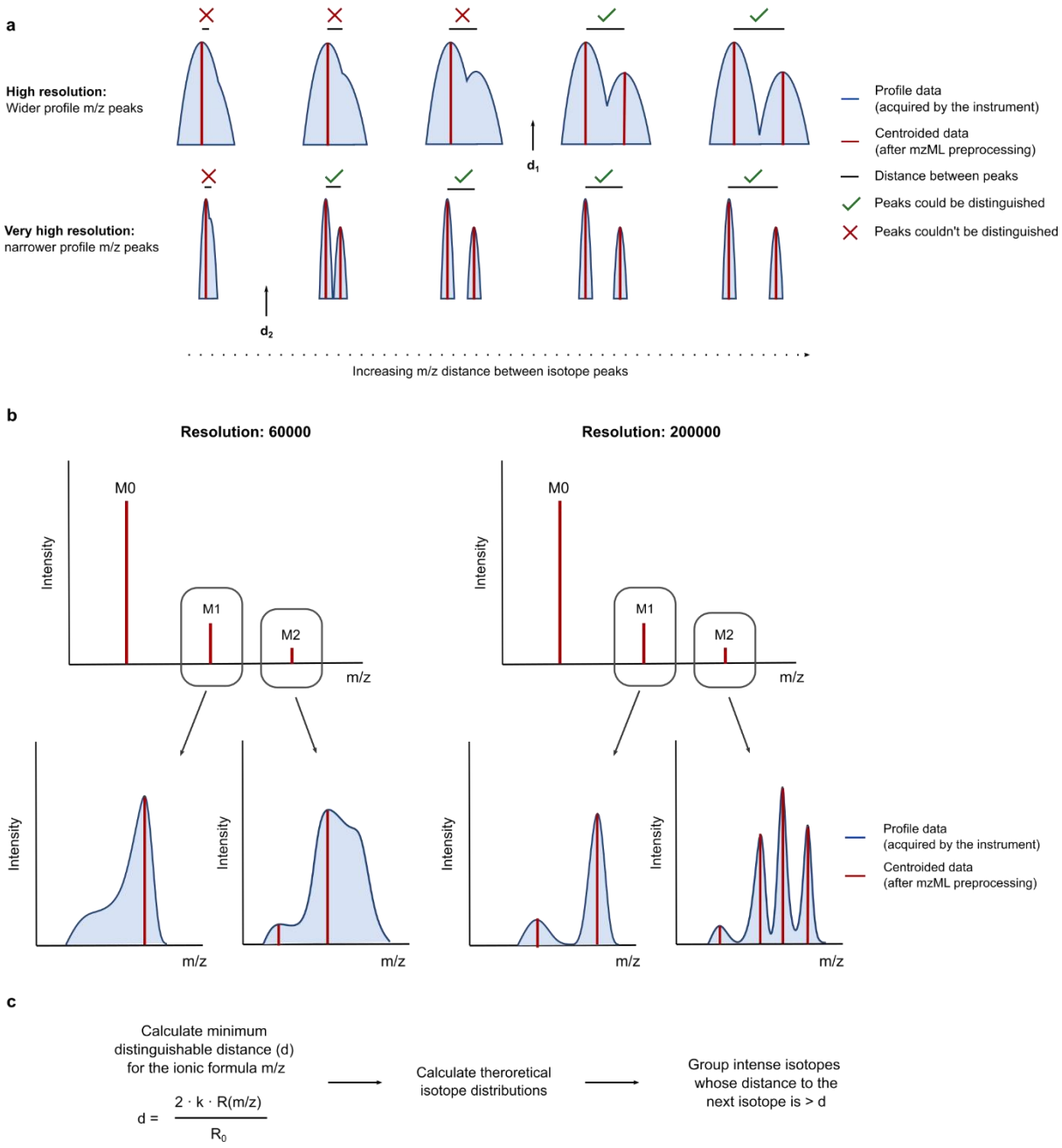

Supplementary Figure S1. Resolution-based isotopic envelope calculation. a) The MS resolution is inversely proportional to the peak width of the acquired signals. When preprocessing raw MS1 data, a centroidization algorithm performs a peak-picking on a continuous profile signal (blue), yielding discrete, centroided signals (red). As resolution increases, the minimal distance to distinguish two adjacent peaks decreases ($d_2 < d_1$). b) In practice, this implies that, when acquiring data at lower resolutions, certain isotope signals are masked by close, more intense signals c) By calculating a resolution-based parameter d, HERMES can estimate which close isotopologues can be distinguished in the acquired profile MS1 data and therefore present in the centroided data (See Algorithm 1).

639

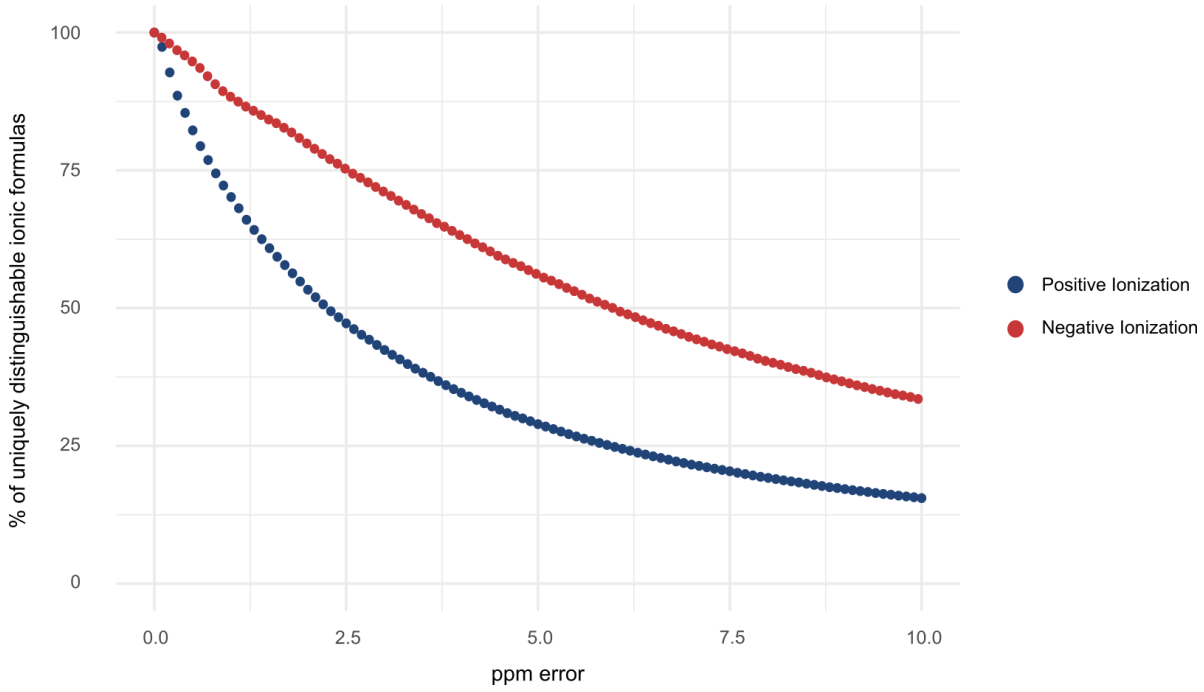

Supplementary Figure S2. Distribution of uniquely distinguishable ionic formulas: Ionic formula collisions from the NORMAN database (24,696 unique molecular formulas). Blue: Positive ionization taking $[M+H]^+$, $[M+Na]^+$, $[M+K]^+$, $[M+NH4]^+$ and $[M]^+$ adducts. Red: Negative ionization taking $[M-H]^-$ and $[M+Cl]^-$ adducts. As the ppm error of the instrument increases, the larger the percentage of overlapping ionic formulas. The shape of the curve is closely related to the number of possible ionic formulas (distinct combinations of formulas-adducts) that are considered: the more ionic formulas, the larger the probability of overlaps.

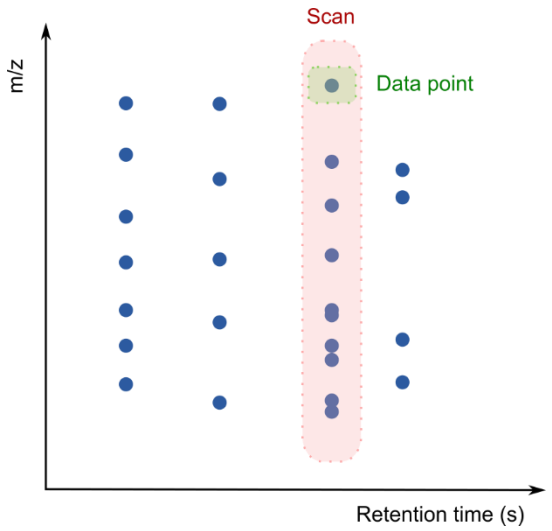

Supplementary Figure S3: Difference between the terms *scan* and *data point*. A *data point* is defined as a triplet {m/z, Retention Time, Intensity}, while a *scan* is the set of data points with the same retention time. A different concept is that of a *feature*, which is an abstract

concept defined as the m/z and retention time interval (composed of multiple scans) where a peak has been detected in one or multiple samples.

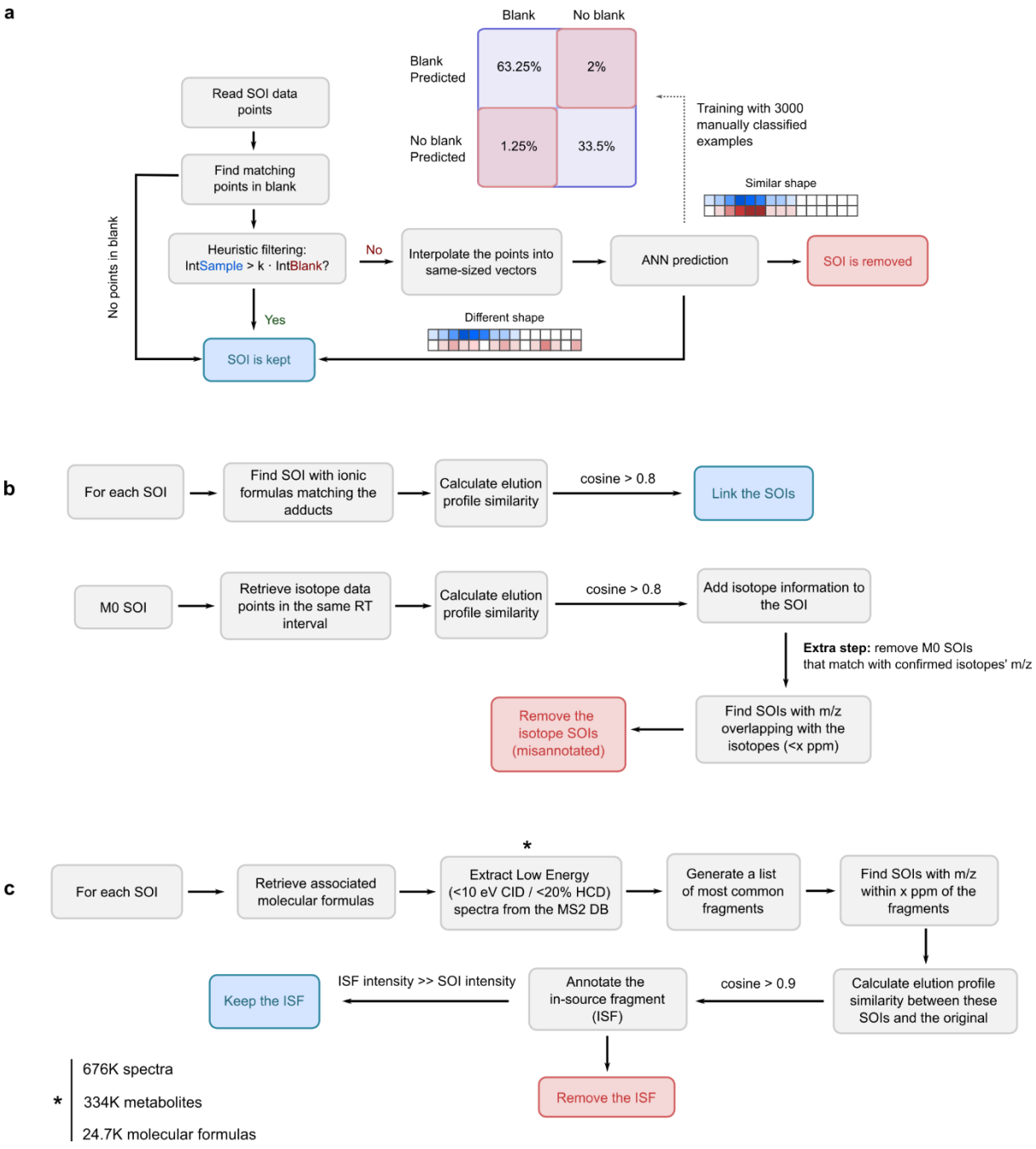

Supplementary Figure S4. Schematic workflow of the different filtering steps in Hermes. a) Artificial neural network (ANN) for blank subtraction. b) Adduct and isotopologue grouping according to the similarity of their elution profiles. c) In-source fragment annotation, by using publicly available low-energy MS/MS data.

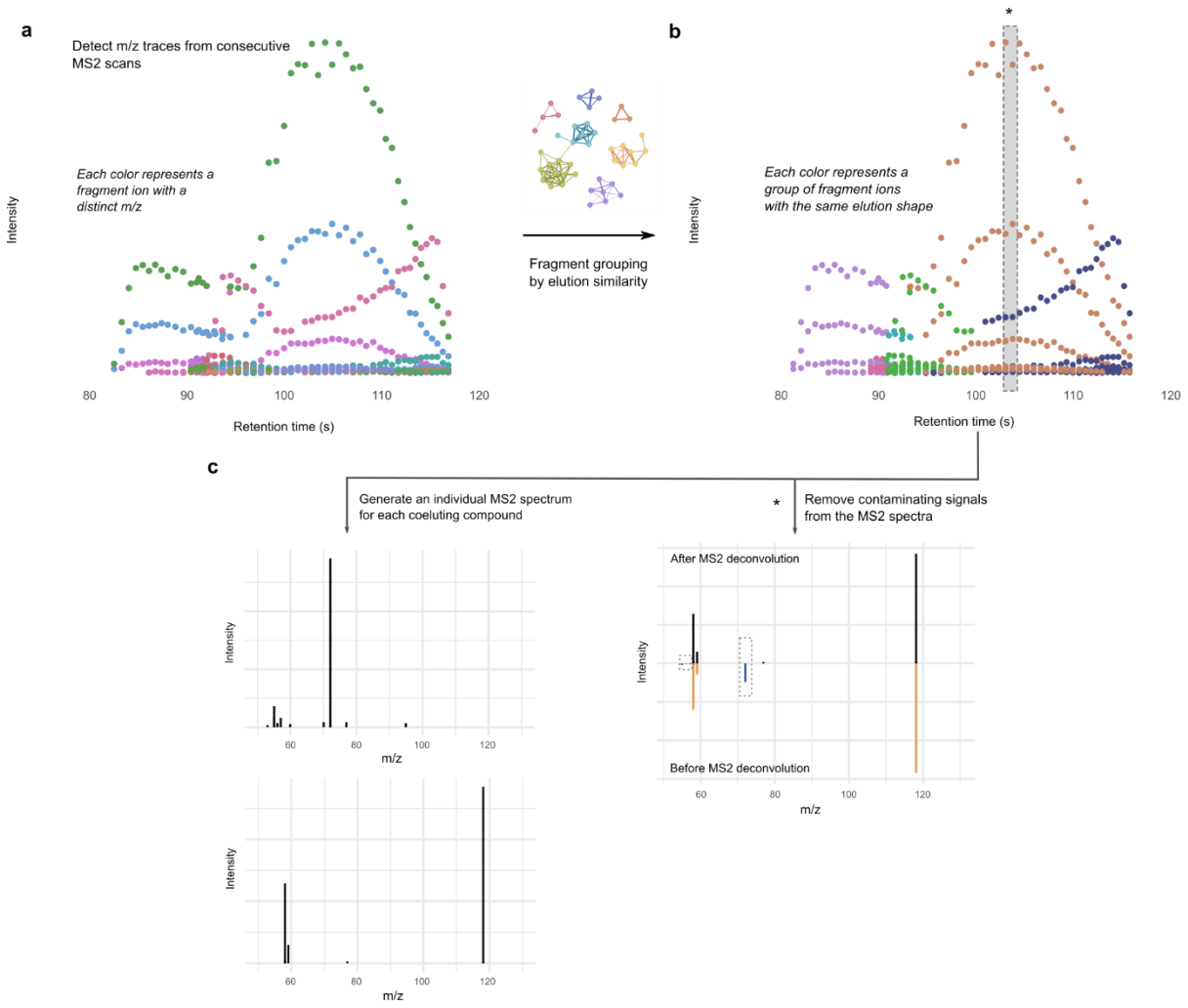

Supplementary Figure S5. Continuous MS2 acquisition resolves co-eluting ionic species by comparing their fragment elution profile. a) All fragment ions from continuous MS2 scans are grouped according to their m/z. b) A loose peak-picking algorithm is applied and the resulting peaks are grouped according to their elution profiles, generating a similarity network that is split by a greedy clustering algorithm. c) This grouping yields a curated MS2 spectra for each coeluting species (see Algorithm 3). (*) The shaded slice shows the impact of the algorithm on the resulting MS2 spectral quality. The delineated fragments in blue have a different elution pattern from the rest and would contaminate the MS2 spectra if only one scan was acquired at the top of the peak. The grouping performed by HERMES confidently removes the contaminant ions and separates each group of fragments according to their elution.

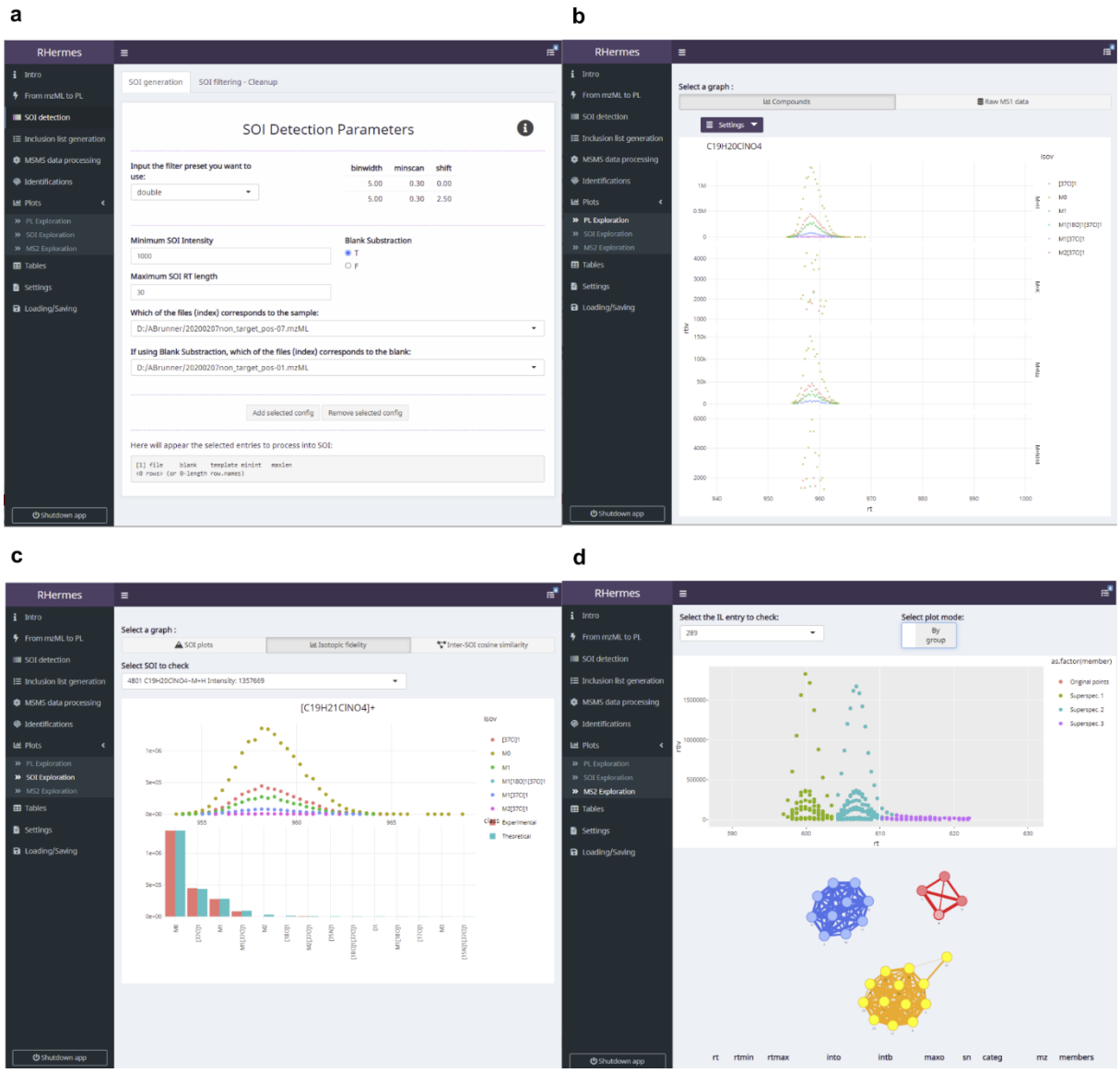

Supplementary Figure S6. **HERMES R Graphical User Interface (GUI).** a) Point-and-click selection of SOI detection parameters, with detailed explanations on their usage and optimal values. b) Visualization of isotopic profiles of different adducts of the same formula. Formulas can be inputted directly or inferred from the name of a selected compound. c) Isotopic fidelity exploration of selected SOIs. d) Visualization of the continuous MS2 deconvolution step. Users can check the fragment ion elution profiles from each inclusion list entry and how they are interconnected in the corresponding profile similarity network.

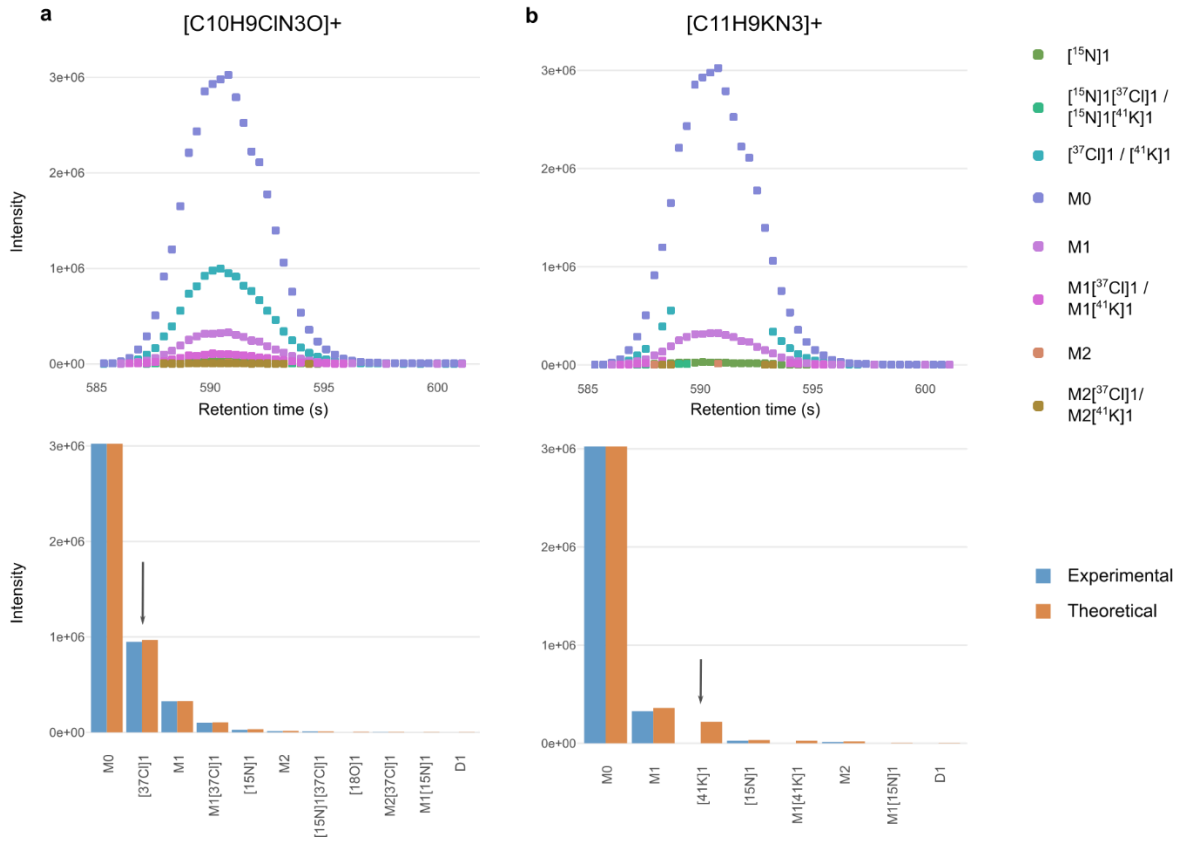

685

686

687 **Supplementary Figure S7**. **Discrimination of SOIs based on isotopic fidelity**. a) $[M+H]^+$
688 ion of chloridazon and b) $[M+K]^+$ ion of 2-Amino-alpha-carboline overlapping at 0.27 ppm. The
689 arrows indicate the characteristic [^{37}Cl] isotopologue present in chloridazon and the [^{41}K]
690 isotopologue absent in 2-Amino-alpha-carboline. The absence of characteristic isotopologue
691 signals (Cl, Br, K, etc.) in an intense SOI results in a low isotopic fidelity score and its removal.

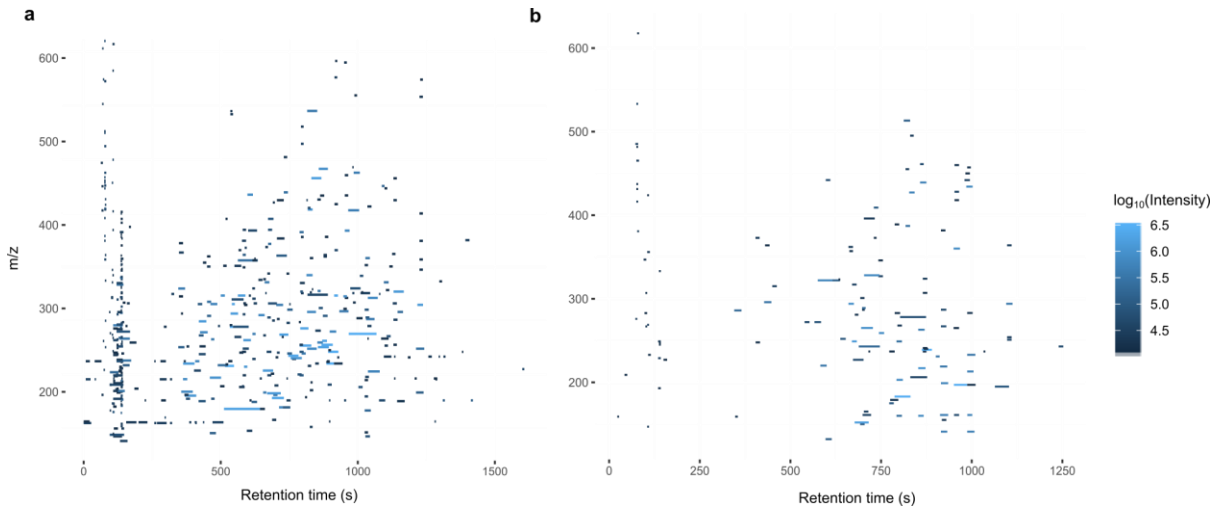

Supplementary Figure S8. Distribution of inclusion list entries of surface water in a) positive and b) negative ionization mode after blank subtraction. The entries are coloured according to their intensity values.

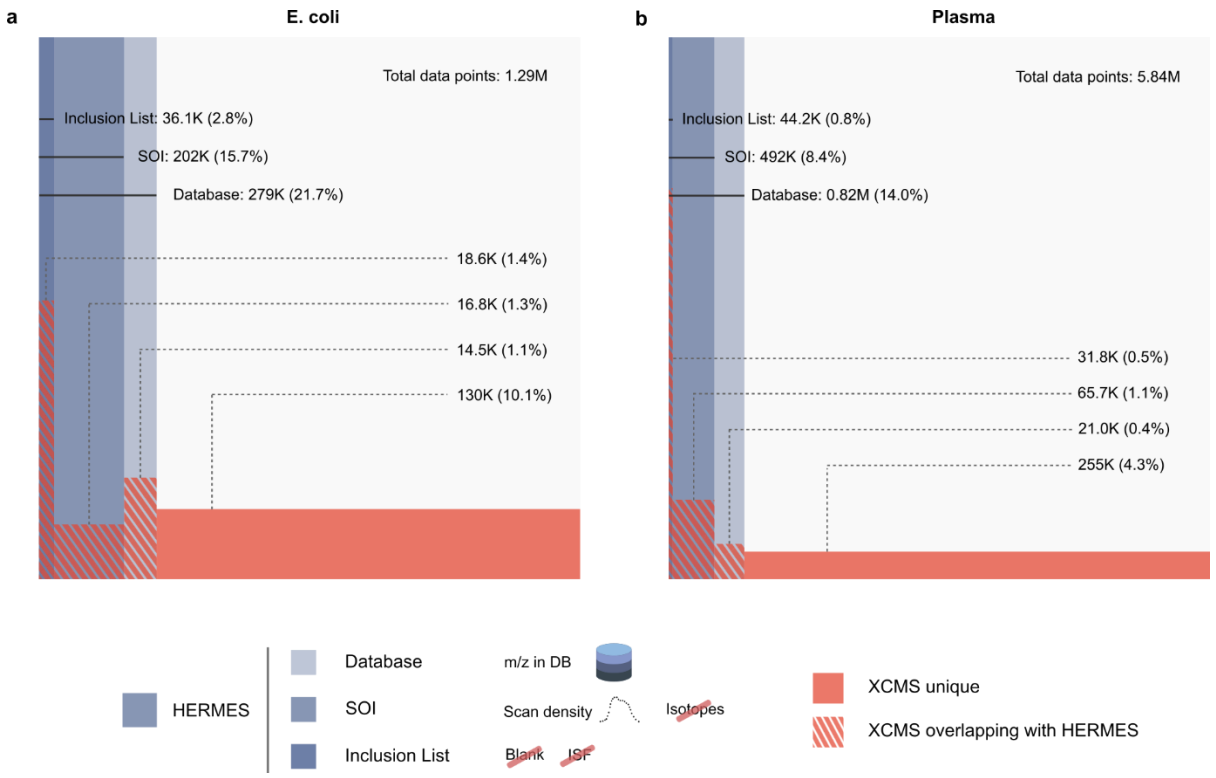

Supplementary Figure S9. **Venn-like diagram of the distribution of negative ionization LC/MS1 data points in different steps of the HERMES workflow and XCMS peak-associated points**. a) *E. coli* and b) human plasma extract. Database: data points that match any m/z from the ionic formula database (including isotopes). SOI: monoisotopic (M0)-annotated data points that are present in an unfiltered SOI list. Inclusion List: data points present in a filtered SOI list (including blank subtraction, isotopic filter and ISF removal steps). Percentages refer to the total number of LC/MS1 data points.

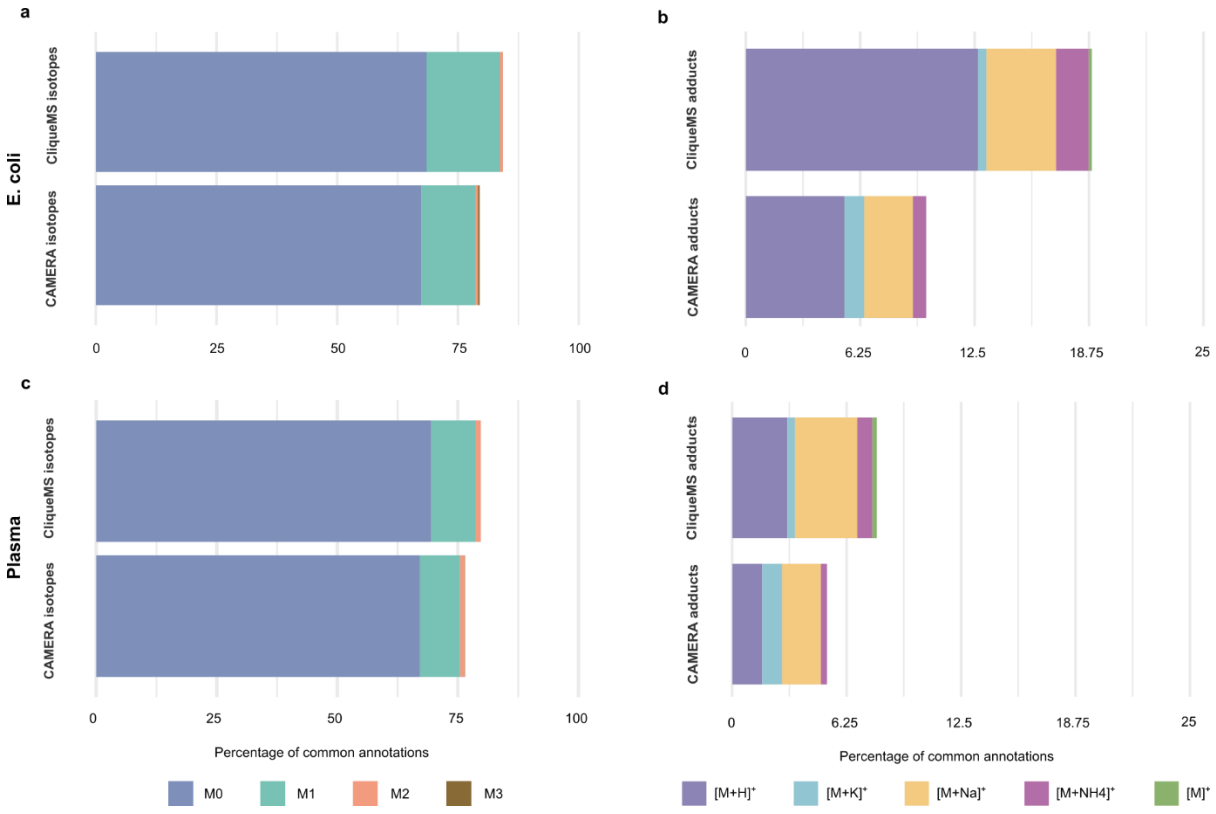

Supplementary Figure S10: Comparing LC/MS1 annotation performance with CAMERA and CliqueMS. Positive ionization data. a) and b) E. coli, c) and d) human plasma extract. Percentages refer to the set of datapoints annotated by HERMES and were detected as a peak by XCMS (see Online Methods for parameters used). The isotope annotation overlap (a and c) was high, due primarily to M0 annotations. On the other hand, adduct annotation overlap (b and d) was markedly low (<20% of datapoints matched the annotation).

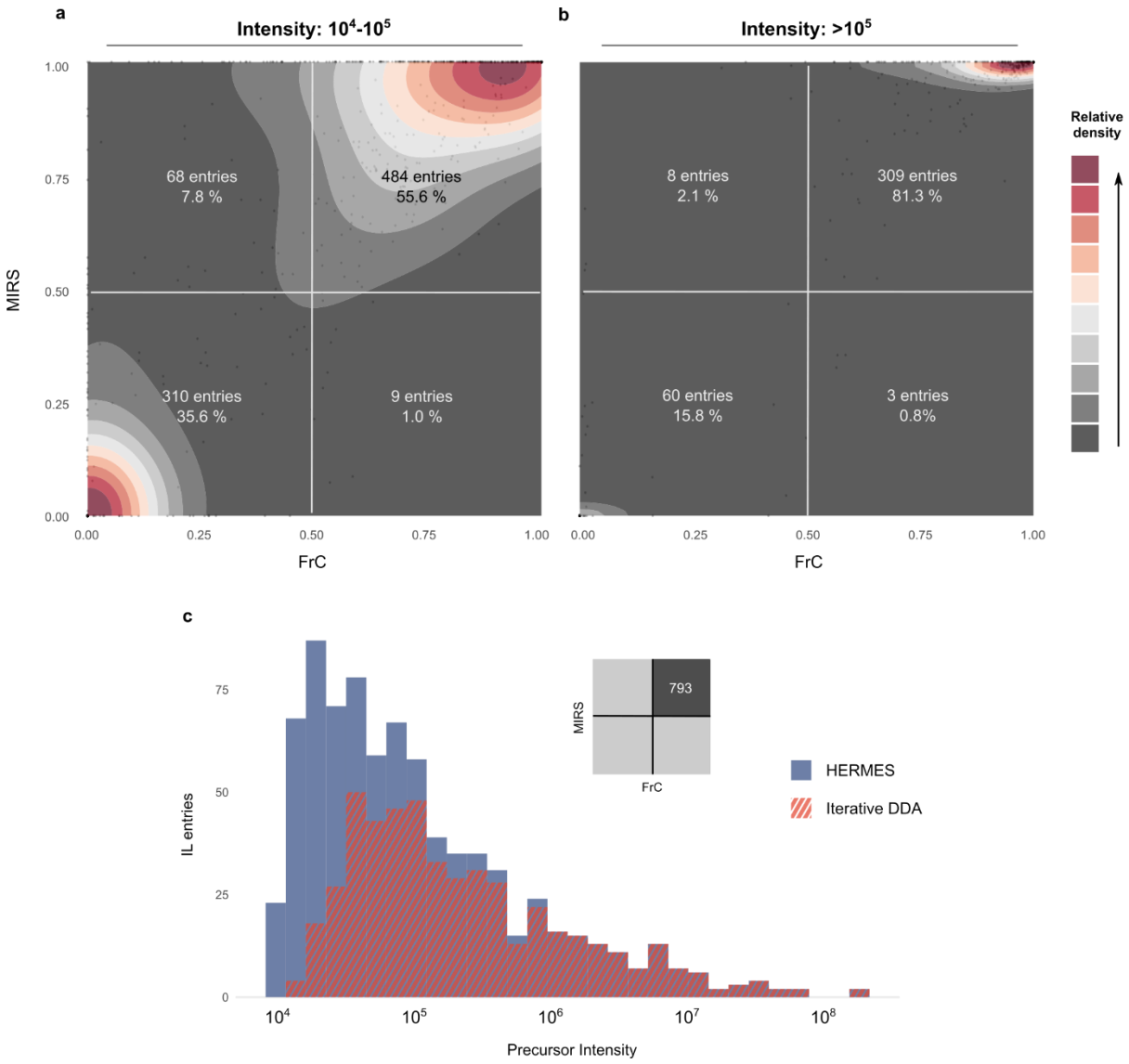

Supplementary Figure S11. ^{13}C-enrichment distribution according to the precursor intensity. a) and b) ^{13}C-enriched metabolites (FC and MIRS > 0.5) are mainly associated with abundant ions (intensity >10^5), while unlabeled precursors (FC and MIRS < 0.5) relate more frequently to low abundant ions (intensity between 10^4-10^5). c) ^{13}C-labeled precursors in iterative DDA corresponded to highly abundant ions that were also covered by Hermes. However, 56% of labelled low abundant ions were not covered by the iterative DDA.

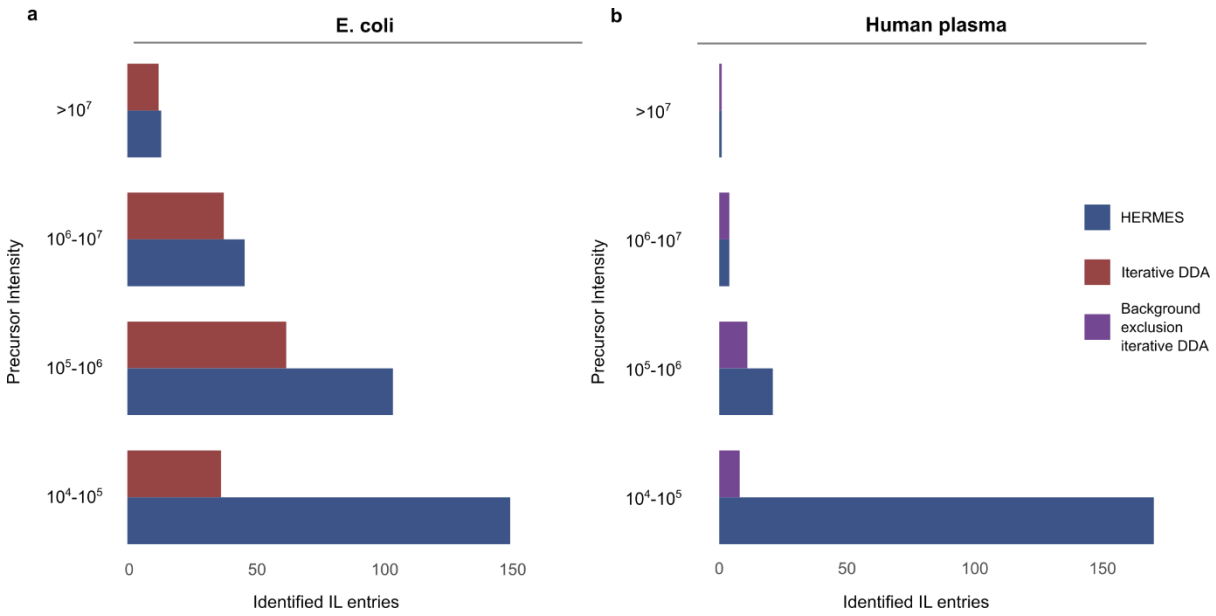

Supplementary Figure S12. **Identified inclusion list entries according to the MS1 precursor intensity in negative ionization data.** An inclusion list entry is considered identified if at least one MS2 scan associated with it has a compound hit in the reference MS2 database with either cosine score > 0.8 (in-house database from MassBankEU, MoNA, Riken and NIST14 spectra), or Match > 90 and Confidence > 30 (mzCloud). a) *E. coli* extract. b) Human plasma extract.

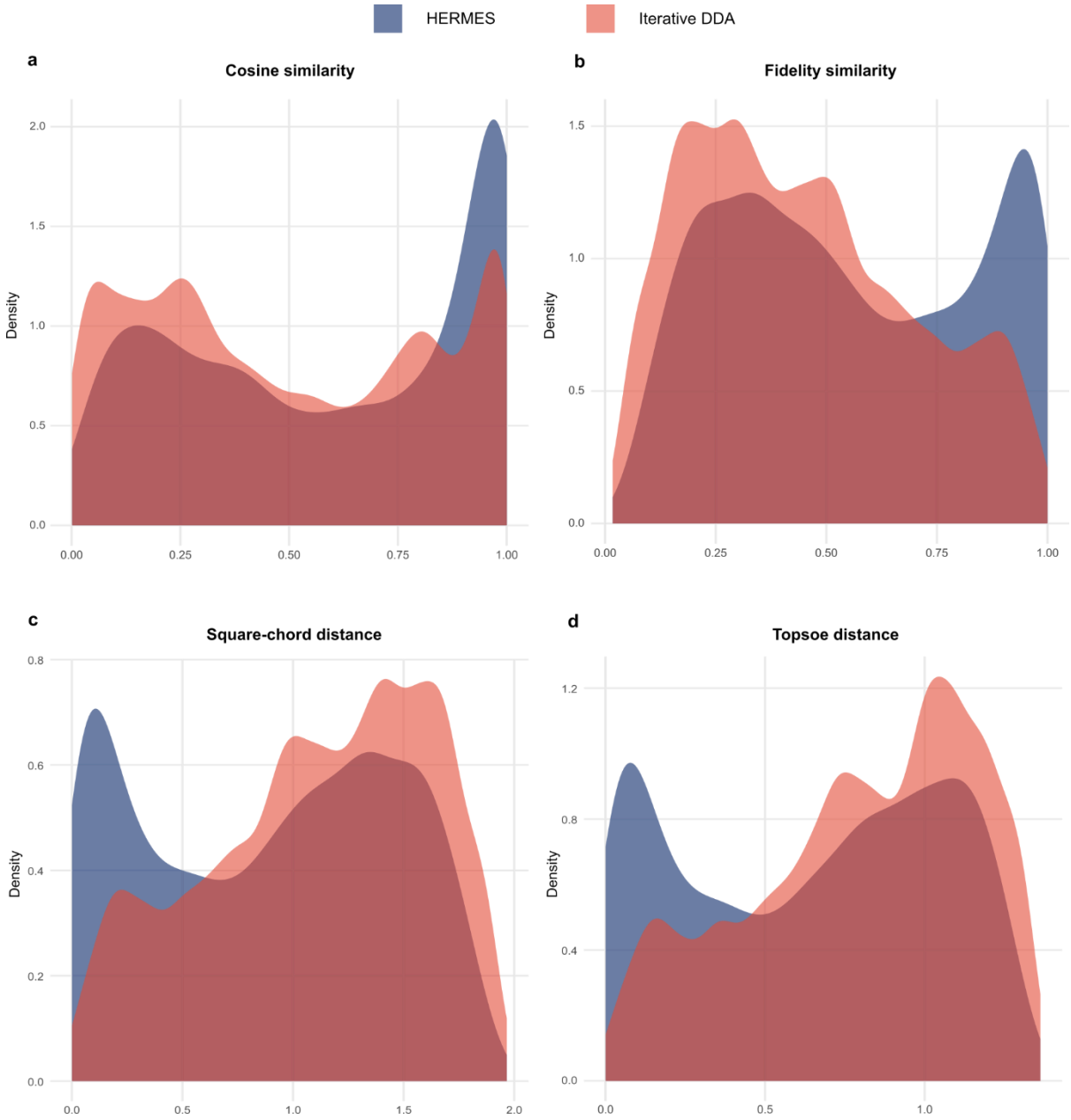

Supplementary Figure S13. Alternative spectral similarity algorithms and spectrum-spectrum match scores. a) Cosine similarity distribution b) Fidelity similarity distribution. c) Square-chord distance distribution. d) Topsoe distance distribution. A density estimation was calculated and normalized so that the integral of the curve equals 1. HERMES spectra showed higher similarity scores (a and b) and lower spectral distances (c and d) than DDA spectra.

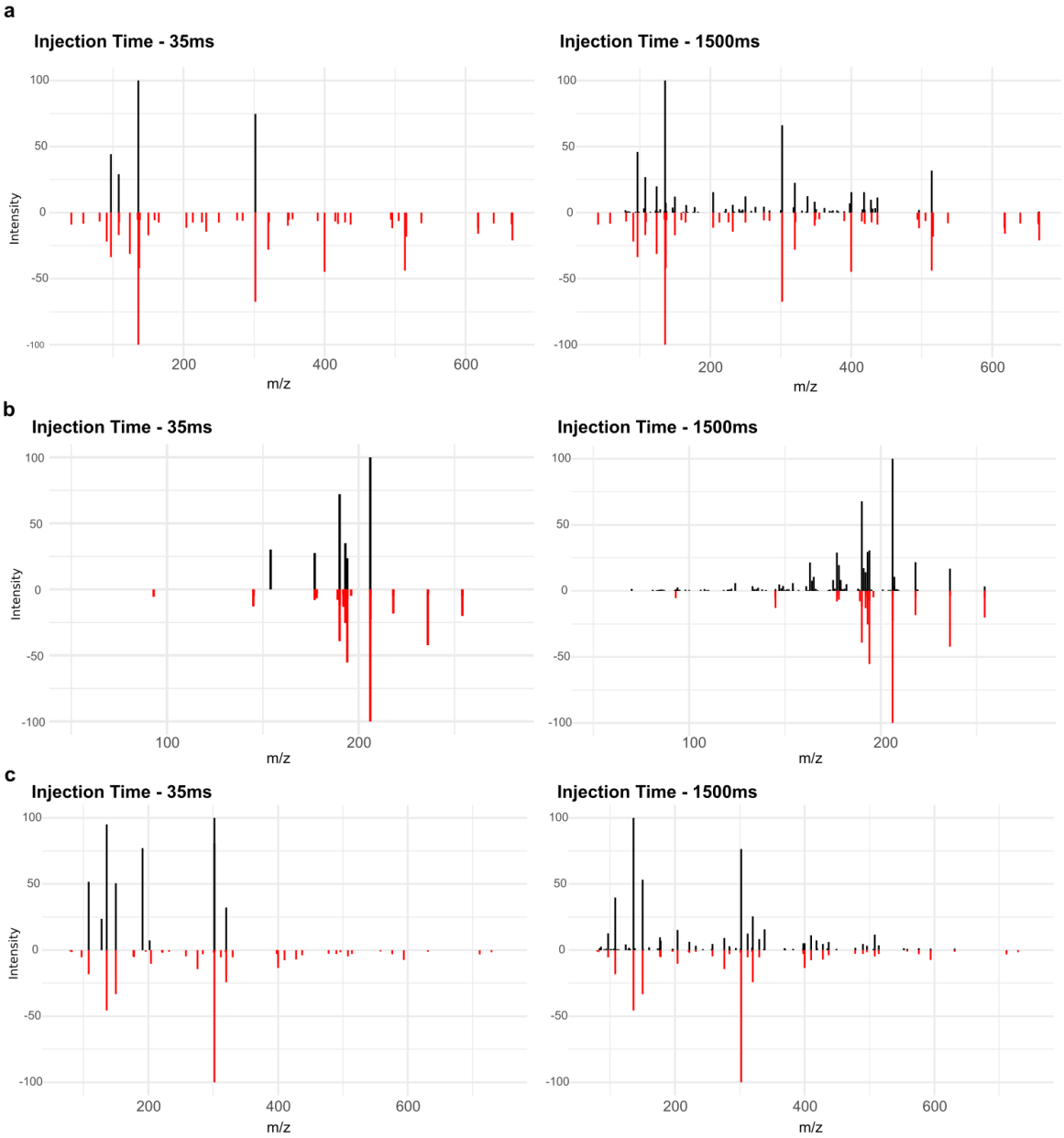

Supplementary Figure S14. **Injection time comparison (35 ms vs 1,500 ms)**. Experimental MS2 spectra (black) of a) NADH, b) Biopterin and c) NADPH against library spectra (red). All precursor ions had an intensity below 10^5. A higher injection time resulted in richer spectra, with more matching fragments against the reference spectra and overall better matching scores.

Supplementary Tables

Supplementary Table 1. Execution times and RAM usage up to the MS1 annotation step.

Number of files (Source)*	Total size of files (MB)	Number of unique ionic formulas	Used RAM (MB)¥	Execution time#
2 (*E. coli*)	42.4	12,010	604	54s
4 (*E. coli*)	82.2	12,010	937	1 min 27s
8 (*E. coli*)	170	12,010	1,279	2 min 30s
2 (Plasma)	131	212,666	6,134	20 min 17s
4 (Plasma)	257	212,666	6,814	24 min 5s
8 (Plasma)	513	212,666	8,705	44 min 17s

*mzML files must be centroided. ¥Difference in RStudio RAM usage before and after processing the files. #Until *Peaklist generation* (MS1 annotation) step.

Supplementary Table 2. List of spiked compounds.

Compound name	Formula	Adduct	m/z	RT (min)
1-(3,4-dichlorophenyl)-3-methylurea	$C_8H_8Cl_2N_2O$	$[M+H]^+$	219.0086	14.28
1-(3,4-Dichlorphenyl)-urea	$C_7H_6Cl_2N_2O$	$[M+H]^+$	204.9930	13.29
2,4-Dichloroaniline	$C_6H_5Cl_2N$	$[M+H]^+$	161.9872	16.77
2,6-dichlorobenzamide (BAM)	$C_7H_5Cl_2NO$	$[M+H]^+$	189.9821	8.18
2-aminoacetophenone	C_8H_9NO	$[M+H]^+$	136.0757	11.93
Atrazine	$C_8H_{14}ClN_5$	$[M+H]^+$	216.1011	14.54
Azinphos-methyl	$C_{10}H_{12}N_3O_3PS_2$	$[M+H]^+$	318.0131	17.17
Bezafibrate	$C_{19}H_{20}ClNO_4$	$[M+H]^+$	362.1154	15.95
Bromacil	$C_9H_{13}BrN_2O_2$	$[M+H]^+$	261.0233	12.43
Caffeine	$C_8H_{10}N_4O_2$	$[M+H]^+$	195.0877	6.83
Carbamazepine	$C_{15}H_{12}N_2O$	$[M+H]^+$	237.1022	13.27
Carbendazim	$C_9H_9N_3O_2$	$[M+H]^+$	192.0768	6.38
Chlorpyrifos-ethyl	$C_9H_{11}Cl_3NO_3PS$	$[M+H]^+$	349.9336	23.34
Chlortoluron	$C_{10}H_{13}ClN_2O$	$[M+H]^+$	213.0789	14.31
Chloridazon	$C_{10}H_8ClN_3O$	$[M+H]^+$	222.0429	9.79
DEET	$C_{12}H_{17}NO$	$[M+H]^+$	192.1383	14.83
Desethylatrazine	$C_6H_{10}ClN_5$	$[M+H]^+$	188.0698	9.78
Desisopropyl Atrazine	$C_5H_8ClN_5$	$[M+H]^+$	174.0541	7.69

Diclofenac	$C_{14}H_{11}Cl_2NO_2$	$[M+H]^+$	296.0240	18.37
Dimethenamid-p	$C_{12}H_{18}ClNO_2S$	$[M+H]^+$	276.0820	17.37
Dimethoate	$C_5H_{12}NO_3PS_2$	$[M+H]^+$	230.0069	10.29
Dimethomorph (isomer 1)	$C_{21}H_{22}ClNO_4$	$[M+H]^+$	388.1310	16.18
Dimethomorph (isomer 2)	$C_{21}H_{22}ClNO_4$	$[M+H]^+$	388.1310	16.59
Diuron	$C_9H_{10}Cl_2N_2O$	$[M+H]^+$	233.0243	15.07
Ethofumesate	$C_{13}H_{18}O_5S$	$[M+H]^+$	287.0948	18.48
Phenazone	$C_{11}H_{12}N_2O$	$[M+H]^+$	189.1022	8.66
Isoproturon	$C_{12}H_{18}N_2O$	$[M+H]^+$	207.1492	14.93
Linuron	$C_9H_{10}Cl_2N_2O_2$	$[M+H]^+$	249.0192	17.24
Metazachlor	$C_{14}H_{16}ClN_3O$	$[M+H]^+$	278.1055	15.87
Metobromuron	$C_9H_{11}BrN_2O_2$	$[M+H]^+$	259.0077	15.60
Metolachlor	$C_{15}H_{22}ClNO_2$	$[M+H]^+$	284.1412	18.92
Metoprolol	$C_{15}H_{25}NO_3$	$[M+H]^+$	268.1907	9.46
Metoxuron	$C_{10}H_{13}ClN_2O_2$	$[M+H]^+$	229.0738	11.94
Metribuzin	$C_8H_{14}N_4OS$	$[M+H]^+$	215.0961	13.19
Monuron	$C_9H_{11}ClN_2O$	$[M+H]^+$	199.0633	12.66
Nicosulfuron	$C_{15}H_{18}N_6O_6S$	$[M+H]^+$	411.1081	12.24
Pentoxifylline	$C_{13}H_{18}N_4O_3$	$[M+H]^+$	279.1452	9.46
Pirimicarb	$C_{11}H_{18}N_4O_2$	$[M+H]^+$	239.1503	9.11
Simazine	$C_7H_{12}ClN_5$	$[M+H]^+$	202.0854	12.50
Sulfadimidine	$C_{12}H_{14}N_4O_2S$	$[M+H]^+$	279.0910	8.38
Sulfamethoxazole	$C_{10}H_{11}N_3O_3S$	$[M+H]^+$	254.0594	10.69
Terbuthylazine	$C_9H_{16}ClN_5$	$[M+H]^+$	230.1167	16.85
Tetraglyme	$C_{10}H_{22}O_5$	$[M+H]^+$	223.1540	7.78
Triethyl Phosphate	$C_6H_{15}O_4P$	$[M+H]^+$	183.0781	10.94
Triphenylphosphine Oxide	$C_{18}H_{15}OP$	$[M+H]^+$	279.0933	15.34
Tri-n-butyl-phosphate	$C_{12}H_{27}O_4P$	$[M+H]^+$	267.1720	20.52
Tri-(2-chloroisopropyl)Phosphate	$C_9H_{18}Cl_3O_4P$	$[M+H]^+$	327.0081	17.24
Tris(2-chloroethyl)Phosphate (TCEP)	$C_6H_{12}Cl_3O_4P$	$[M+H]^+$	284.9612	14.26
2.4.6-trichlorophenol	$C_6H_3Cl_3O$	$[M+H]^-$	194.9177	17.77
2.4-dichlorophenol	$C_6H_4Cl_2O$	$[M+H]^-$	160.9566	16.52
2,4-dichlorophenoxyacetic Acid (2,4-D)	$C_8H_6Cl_2O_3$	$[M+H]^-$	218.9621	15.25
2.4-dinitrophenol	$C_6H_4N_2O_5$	$[M+H]^-$	183.0047	13.21

(4-chloro-2-methylphenoxy)-Acetic Acid (MCPA)	$C_9H_9ClO_3$	$[M+H]^-$	199.0168	15.31
Bentazon	$C_{10}H_{12}N_2O_3S$	$[M+H]^-$	239.0496	14.44
Dichlorprop (2.4-DP)	$C_9H_8Cl_2O_3$	$[M+H]^-$	232.9778	16.52
Mecoprop (MCPP)	$C_{10}H_{11}ClO_3$	$[M+H]^-$	213.0324	16.53
p,p-sulfonyldiphenol	$C_{12}H_{10}O_4S$	$[M+H]^-$	249.0227	11.21
N-acetyl sulfamethoxazole	$C_{12}H_{13}N_3O_4S$	$[M+H]^+$	296.0700	11.06
Metolachlor ESA	$C_{15}H_{23}NO_5S$	$[M+H]^+$	330.1370	11.24
10,11-dihydro-10,11-dihydroxy Carbamazepine	$C_{15}H_{14}N_2O_3$	$[M+H]^+$	271.1077	7.55
Gabapentin	$C_9H_{17}NO_2$	$[M+H]^+$	172.1332	6.45
Hydrochlorothiazide	$C_7H_8ClN_3O_4S_2$	$[M+H]^-$	295.9572	7.20
Desfenylchloridazon	$C_4H_4ClN_3O$	$[M+H]^+$	146.0116	2.25
Lamotrigine	$C_9H_7Cl_2N_5$	$[M+H]^+$	256.0151	9.36
Metazachlor ESA	$C_{14}H_{17}N_3O_4S$	$[M+H]^+$	324.1013	9.19
N-formyl-4-aminoantipyrine	$C_{12}H_{13}N_3O_2$	$[M+H]^+$	232.1081	7.12
N-acetyl-4-aminoantipyrine	$C_{13}H_{15}N_3O_2$	$[M+H]^+$	246.1237	7.08
Metazachlor OA	$C_{14}H_{15}N_3O_3$	$[M+H]^+$	274.1186	9.32
Sitagliptin	$C_{16}H_{15}F_6N_5O$	$[M+H]^+$	408.1254	10.27
Valsartan Acid	$C_{14}H_{10}N_4O_2$	$[M+H]^+$	267.0877	11.78
Gabapentin-lactam	$C_9H_{15}NO$	$[M+H]^+$	154.1226	11.22
HMMM	$C_{15}H_{30}N_6O_6$	$[M+H]^+$	391.2300	13.24
Candesartan	$C_{24}H_{20}N_6O_3$	$[M+H]^+$	441.1670	14.37
Irbesartan	$C_{25}H_{28}N_6O$	$[M+H]^+$	429.2397	14.13
Valsartan	$C_{24}H_{29}N_5O_3$	$[M+H]^+$	436.2343	16.51
Sebutylazine	$C_9H_{16}ClN_5$	$[M+H]^+$	230.1167	16.20
Telmisartan	$C_{33}H_{30}N_4O_2$	$[M+H]^+$	515.2442	14.07
Cetirizine	$C_{21}H_{25}ClN_2O_3$	$[M+H]^+$	389.1627	23.33
1-H-benzotriazole	$C_6H_5N_3$	$[M+H]^+$	120.0556	7.92
4-methyl-1H-benzotriazole	$C_7H_7N_3$	$[M+H]^+$	134.0713	9.94
5-methyl-1H-benzotriazole	$C_7H_7N_3$	$[M+H]^+$	134.0713	10.07
5,6-dimethyl-1H-benzotriazole	$C_8H_9N_3$	$[M+H]^+$	148.0869	11.52
5-chloro-1H-benzotriazole	$C_6H_4ClN_3$	$[M+H]^+$	154.0167	11.30
2-aminobenzothiazole	$C_7H_6N_2S$	$[M+H]^+$	151.0324	6.43
2-hydroxybenzothiazole	C_7H_5NOS	$[M+H]^+$	152.0165	11.59

2-(methylthio)benzothiazole	$C_8H_7NS_2$	$[M+H]^+$	182.0093	17.38

Supplementary Material: Algorithms

Algorithm 1: Resolution-adapted isotopic envelope calculation

Input: Ionic formula f, corresponding m/z, instrument resolution R at m/z = 200, separation threshold k

Output: List of resolvable isotopes I

$R' = R\ (m/z)$ // Estimate instrument resolution for the ionic formula m/z

$d = 2 \cdot k \cdot R'$ // Calculate minimum resolvable m/z distance *d*

$I_{th} = iso\_pattern(f)$ // Calculate theoretical isotopic pattern

$N_{cluster}$ = Number of isotope clusters in I_{th} such that $dist(i,j) < 0.1\ Da$,$\forall\ i,j \in Cluster$

For $cluster$ from 1 to $N_{cluster}$:

    iso_{mz} = sort (mz_i) $\forall i \in cluster$

    if any $(iso_{mz} > d)$: // If there's more than one distinguishable isotope

        Split cluster into groups G such that: $\forall i,j \in G \quad dist(i,j) < d$

        For each $group$ in G:

            Add the isotope with highest intensity in $group$ to I

    Else:

        Add the isotope with highest intensity in $cluster$ to I

Return I

Algorithm 1: By considering the instrumental resolution, this algorithm can adaptively annotate isotopes according to the MS1 acquisition settings. The idea is to extend the definition of chromatographic peak resolution (which compares peaks RTs and widths) to the m/z profiles of isotope peaks and infer whether the centroidization algorithm (frequently used in mzML file pre-processing) can split them into separate data points (see Supplementary Figure 1). To do this, the algorithm (a) estimates the instrument *local* resolution for a particular ionic formula based on a reference resolution, (b) calculates the minimum distinguishable distance d for the centroidization algorithm, (c) calculates a theoretical isotopic envelope and (d) finds all groups of isotopes with distances < d.

Algorithm 2: Scans of Interest (SOI) detection

Input: Annotated data points matrix $D = \{RT,\ intensity\}$, retention time bin width bw, minimum intensity I_{min}, acquired scans header h, minimum scan density (%) ρ, minimum chaos score C_{min}

Output: List of SOIs SOI_{list}

$D' = filter(D,\ intensity > I_{min})$

// Set RT bins

$B_{start} = [0,\ bw,\ 2 \cdot bw, \dots]\ ;\ B_{end} = [bw,\ 2 \cdot bw,\ 3 \cdot bw, \dots]$

// Count number of acquired scans in each RT bin

$Thr = [\ B_{start} \leq\ h_{RT} \leq B_{end}]\ \cdot \rho$

For each bin:

    N_{bin} = $B_{start}[bin]\ \leq D'_{RT} \leq B_{end}[bin]$ // Count annotated data points in the bin

    $\phi_{bin} =\ N_{bin} > Thr_{bin}$ // Determine whether there are enough data points

$\sigma =\ S(\phi_{bin})$ // Find all 1D-connected subsets in ϕ_{bin}

For each $element$ in σ:

    Calculate ρ_{chaos} with the $element$ intensity vector (see Algorithm 4)

    If $\rho_{chaos} > C_{min}$:

        Add $element$ information to the SOI_{list} (start, end, intensity, annotation …)

Return SOI_{list}

Algorithm 2: The SOI detection algorithm establishes a new way of detecting peaks without imposing a gaussian peak-shape on the data. By using a moving window to calculate an average scan density, the algorithm is robust against missing data points (which are frequent in low-intensity signals). SOIs are detected from an already annotated set of datapoints – defined by the considered formulas and adducts– so the resulting SOIs bypass the limitations of current annotation methods (mainly, the requirement of adduct and/or isotope peaks to annotate).

Algorithm 3: Continuous MS2 scan deconvolution

Input: Continuously acquired MS2 scans S from a common precursor m/z, instrument ppm error ppm

Output: Deconvoluted MS2 spectra

// Mass trace detection

For each $scan$ in S:

    Match the scan m/z to those of a trace list T

    If there's a match:

        Extend the trace

    If there are no matches:

        Start a new trace and add the scan

Split traces with RT gaps > 3s

Run *Centwave* peak detection algorithm on each individual trace

// Information propagation based on elution profile similarity

For each trace t detected as a peak:

    For each trace t' **not** detected as a peak:

        Calculate the Pearson correlation r between t and t'

        If $r > 0.8$:

            Trim t' RT interval to match t

            Consider t' as a peak from now on

Repeat previous loop until no more peaks are detected

// Network analysis

Calculate cosine similarities between each trace, generating a similarity matrix M

Generate a network N from M

Find all connected subgraphs in N

For each subgraph:

    Apply a greedy partitioning algorithm.

    If the modularity resulting from the partition is > x:

        Split the subgraph according to the partition

For each resulting subgraph:

    Retrieve the traces that form the subgraph

    Assemble a MS2 spectrum from the maximum intensities of each trace

Return a list of the assembled MS2 spectra.

Algorithm 3: The MS2 deconvolution algorithm separates fragments from coeluting compounds with a common precursor m/z. A key feature of the algorithm is the use of Centwave peak-picking and the *information propagation* from one fragment mass trace to another applying a Pearson correlation: if a peak is detected with Centwave in one trace (usually the most intense), similarly-shaped, coeluting traces are treated as peaks independently of the peak-picking. This propagation step is particularly useful when most traces are weak and noisy, as they are frequently missed by peak-picking algorithms.

Algorithm 4: 1-dimensional ρ_{chaos} calculation

Input: Vector I of intensities of the data points corresponding to a SOI, number n of intensity thresholds

Output: ρ_{chaos}

$I = \frac{I - \min(I)}{\max(I) - \min(I)}$ // Scale intensity to [0, 1]

For $level$ in 1 to n:

$\tau = level \,/\, n$

$\phi = I > \tau$ // Find all intensities above threshold

$\phi' = \psi(\phi)$ // Fill gaps of length 1

$N_{level_i} = S(\phi')$ // Find all 1D-connected subsets in ϕ'

$\rho_{chaos} = 1 - \frac{\sum_{i=1}^{n} N_{level_i}}{length(I) \cdot n}$

Return ρ_{chaos}

Algorithm 4: The ρ_{chaos} calculated by this algorithm is the 1D equivalent of the ρ_{chaos} applied in MS-imaging software like METASPACE. The objective is to quantify the amount of structure contained in a datapoint intensity vector: when increasing a threshold $level$, a vector of noisy datapoints generates many unconnected sets above the $level$ (low ρ_{chaos}), while well-structured datapoints stay in one/few connected sets (high ρ_{chaos}).